Oil Emissions from Nearshore and Onshore Summerland: Final Report

April 11, 2007

Ira Leifer (UCSB), Ken Wilson, Robin Lewis, and Randy Imai (DFG-OSPR), and John Tarpley (NOAA)

Special Thanks to the Key Participants:
Shane Anderson (UCSB – Diver, Boat Operator)
Victor Blalack (DFG/OSPR - Boat Operator)
Ann Bull (MMS - Diver)
Josh Curtis (DFG/OSPR -T echnical Specialist - Scientist)
Steve Curran (CSLC – Petroleum Drilling Engineer)
Marc Demeo (CSLC - Inspector)
Dave Farrar (UCSB – Diver/Boat Operator
Jorge Gross, (DFG Enforcement - Boat Driver; Diver)
James Hemphill (CSLC – Engineering Manager)
Randy Imai (DFG/OSPR - Boat Operator/GPS Specialist)
Ira Leifer (UCSB - Scientist)
Robin Lewis (DFG/OSPR –Diver/Scientist)
Una Matko (UCSB – Student Assistant)
Chris McCullough (Dept of Conservation -A erial Imagery)
Ken Mayer (DFG – Chief Scientific Branch)
Ray Michalski (DFG/Marine Region – Captain)
Carlton Moore (DFG - Administrator)
Bill Paznokas (Marine Region - Scientist)
Hector Orozco (DFG Enforcement - Boat Operator)
Larry Philip (CSLC - Inspector)
Greg Sanders (Fish and Wildlife -Di ver/Videographer)
Tonya Del Sontro (UCSB, Diver)
Mike Sowby (DFG - EPM1)
Derek Stein (DFG/Marine Region, Biologist)
Ian Taniguchi (DFG/Marine Region – Diver/Biologist)
John Tarpley (DFG/OSPR/NOAA – Diver - Scientist)
Ron Tripe (CSLC - Inspector)
John Ugoretz (DFG/Marine Region – Diver -S cientist)
(USCG Marine Safety Detachment – Santa Barbara)
George Wardlaw (UCSB - Diver)
Ken Wilson (DFG/OSPR - Scientist)

Citation: 2007. Oil emissions from nearshore and onshore Summerland: Final Report. OSPR Technical Publication No. 07- 001. State of California Department of Fish and Game - Office of Spill Prevention and Response. 1700 'K' St. Sacramento, Calif. 95814.

EXECUTIVE SUMMARY

In the mid to late 19th century, coastal and inshore areas of natural seepage often were targeted by prospectors to locate sites for oil production facilities. Inadequate well abandonment procedures left a legacy of leaking oil wells, many in some areas of natural seepage. This has led to recurrent seepage problems, particularly in the Summerland area in southern Santa Barbara County, California. These seepage problems have and continue to cause concern to the public and regulators, and multiple and sometimes-unsuccessful abandonment efforts. This study focused on the repeatedly problematic Treadwell T-10 Well, formerly located on the Treadwell Wharf, where the world's first offshore oil well was drilled in the late 1800s. The study also investigated other nearshore and onshore oil and gas sources in the Summerland beach area.

Studies began in 2001 and continued on an intermittent basis until 2005 and included shore-side, beach, sea-surface, underwater, and aerial surveys and historical research related to oil seepage and its effects on beaches, water, and biota in the Summerland beach area. Efforts included the deployment of specifically designed oil and gas collection devices – tents - at several emission sites at Summerland beach. Although primarily directed at abandoned oil wells/casings in very shallow water at Summerland, California, the methods pioneered for this study and its conclusions are applicable for quantifying oil seepage from abandoned oil facilities and natural seeps in both marine and terrestrial environments.

Key study findings:

Investigation of geological data, historical records and sea surface surveys strongly suggest a fault trend passing through the T-10 Well Site which likely has contributed to the repeated failure of abandonment efforts.

Oil emissions occurred from two vent areas on diametrically opposed sides of the T-10 Well cement/metal cap. Using two oil seep collection tents, which included shipboard video monitoring of oil/gas emissions, quantitative seepage rates were measured at both vents through a tidal cycle. Emissions were well correlated with tides – 98% correlation for oil emissions, and 91% for gas.

Based on the oil emission relationship with tides, total oil emissions were 2.4 liters per day, while total gas emissions were 39 liters per day (at standard temperature and pressure), for a gas to oil ratio of 16 to 1. Thus, most of the black oily bubbles escaping at the seabed, which appeared to be pure oil droplets, actually were primarily gas.

Moreover, changes in the oil to gas ratio were inversely correlated between the two areas of vents at the T-10 Well Site, demonstrating subsurface connectivity between the vents.

Data were further analyzed in terms of an electrical circuit network, which was used to non-invasively infer details of the subsurface seepage. This model suggested that the connection between the two vents occurred quite shallowly, and that the well casing provided a relatively low resistance pathway compared to the pathways around the concrete and metal caisson near the seabed.

Although, observations were consistent with interconnectivity between the Treadwell T-10 Well Site and the S-3 Site, proposed to be at the historical site of the Moore Wharf, they did not prove the hypothesis. Analysis of the gas to oil ratios demonstrated interconnectivity between vents on the north and south sides of the Treadwell T-10 Well Site, and the south of the Treadwell T-10 Well cement and metal cap, validating the experimental approach.

Throughout the multiyear study period, no oiled wildlife was observed in the Summerland beach area.

Three peer-reviewed manuscripts were published based on this research:

Leifer, I and K. Wilson. 2007. Tides and the Emission of Oil and Gas from an Abandoned Oil Well: Nearshore, Summerland, California. *Marine Pollution Bulletin,In Press.*

Leifer, I., and K. Wilson, J. Tarpley, R. Lewis, R. Imai, K. Mayer, and C. Moore. 2005. Factors affecting marine hydrocarbon emissions in an area of natural seeps and abandoned oil wells - Summerland, California. *Proc. Internat. Oil Spill Conf., May 15-19, 2005, Miami, FL*, EIS Digital Publishing, 14718A.

Leifer, I and K. Wilson. 2004. Quantified oil emissions with a video-monitored, oil seep-tent. *Marine Technology Society Journal*, **38(3)**, 44-53.

Key Study Conclusions:

Studies offshore Summerland identified likely locations of faults, trends of natural seepage, and man-made, oil-related facilities. Consideration of the data strongly suggest that the Treadwell T-10 Well, which was abandoned three times, was drilled into a fault zone. Although we have no information on oil and gas emissions from the T-10 Well Site were prior to mid 20th century abandonment efforts, small discharges occur at the site on an intermittent basis. Our findings suggest that any future abandonment efforts are likely to result in similar lack of success, with small-scale seepage eventually becoming evident due to natural seismic-related processes.

Given the shallowness of the reservoir, it is unlikely that large oil emissions will arise from the capped T-10 Well Site or for that matter other recently abandoned area sites in their current condition. A significant increase in aquifer pressure could cause an increase in oil and gas emissions. However, given the shallowness and isolated nature of the oil reservoir, any increases would be small and short-lived, particularly compared to other natural oil sources in the Santa Barbara Channel, specifically, the Coal Oil Point seep field.

One of the important study conclusions was that observer perception can significantly affect perceived emissions of oil, and lead to emission estimates highly divergent from quantitative emission measurements.

Table of Contents

List of Figures

List of Tables

1. INTRODUCTION

Petroleum in the ocean is of enormous concern, affecting the environment, economy, and quality of life for coastal inhabitants. The *NRC* (2003) estimated that during the 1990s, 1,300,000 tons (325 million [M] gallons) of oil entered the oceans annually worldwide. Spills from marine vessels accounted for 100,000 tons (25 M gals), run-off from land 140,000 tons (35 M gals), and pipelines just 12,000 tons (3 M gals). For comparison, natural seeps annually emitted an estimated 600,000 tons (150 M gals) of oil into the ocean, 160,000 tons (40 M gals) of which escaped into North American waters. Natural seepage in California, alone, contributed approximately 20,000 tons (5 M gals) of oil to the ocean. Despite the significance of oil in the ocean, most of its sources remain unquantified, and most details of its fate in the marine environment remain unknown.

Much of the California coastline, from Pt. Conception to Santa Monica, was home to numerous oil piers, platforms, and wells in both nearshore and offshore waters, many of which are now abandoned. A number of these oil facilities were alleged to have been abandoned improperly, posing a threat of leakage (*Grosbard*, 2002). Furthermore, many of these facilities (abandoned and active) are located in regions of natural seepage. In some cases, oil exploitation activities can take advantage of oil migration from deep subsurface reservoirs along faults and fractures to shallower depth strata (e.g., Platform Holly). Of course, in many areas, this migration continues to the seabed and then the ocean surface. This aspect has long been used by oil prospectors in determining where to conduct geotechnical surveys, build piers, drill wells, and place platforms. However, if natural and anthropogenic emissions occur in the same area, they pose to regulatory agencies a complex array of challenges with respect to assessment, regulation, and mitigation. This is particularly important when responsible parties no longer exist and state and/or federal taxpayers could be asked to pay for control, containment, and cleanup.

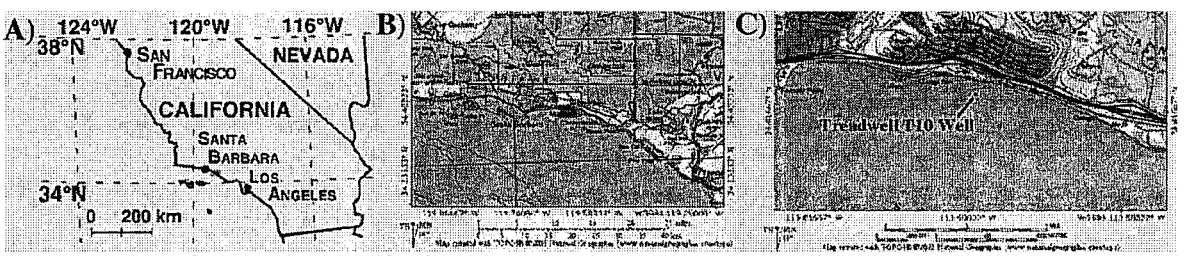

Figure 1. Maps of **A)** Southern California B) Santa Barbara-Ventura area, and **C)** Summerland beach area. Red boxes shows the location of the Summerland beach area. The Treadwell T-10 Well Site is noted in **C)**.

This study's focus relates to abandoned oil wells and natural oil seeps located in shallow (3-m to 7-m) nearshore waters and in the intertidal zone, at Summerland beach, CA (*Leifer and Wilson*, 2004; *Leifer et al.*, 2005). Studies began in 2001 and continued on an intermittent basis until 2005 and included shore-side, beach, sea-surface, underwater, and aerial surveys and historical research. These efforts included the deployment of specifically designed oil and/or oil and gas collection devices at several emission sites at Summerland beach. These studies also sought to understand the magnitude of the effects on beaches and wildlife. Although the field studies primarily were directed at abandoned oil wells/casings in very shallow water at Summerland, California, the methods pioneered for this study and its conclusions are applicable for quantifying oil seepage from abandoned oil facilities and natural seeps in both marine and terrestrial environments.

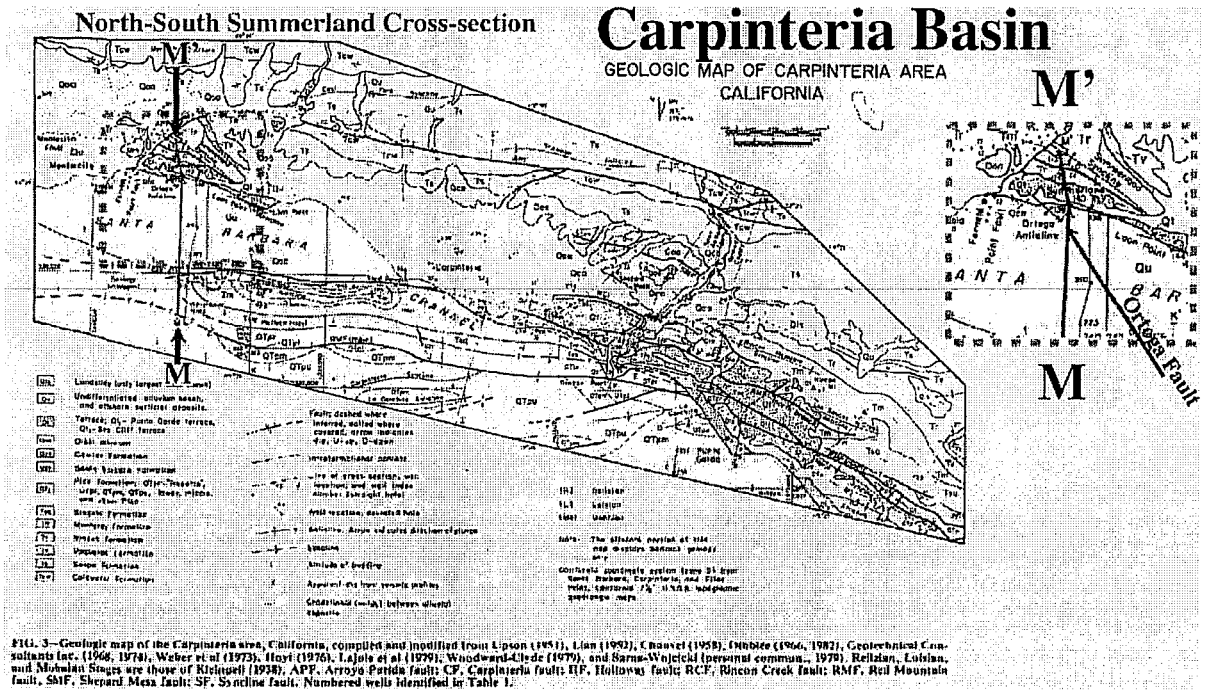

Figure 2. Geologic map of the Carpinteria Basin. MM' shows location of vertical cross section relevant to Summerland. Rectangle covers Summerland study area – enlarged inset shows MM' cross section and Ortega Fault offshore Summerland. Taken from *Jackson and Yeats* (1982; Figure 3).

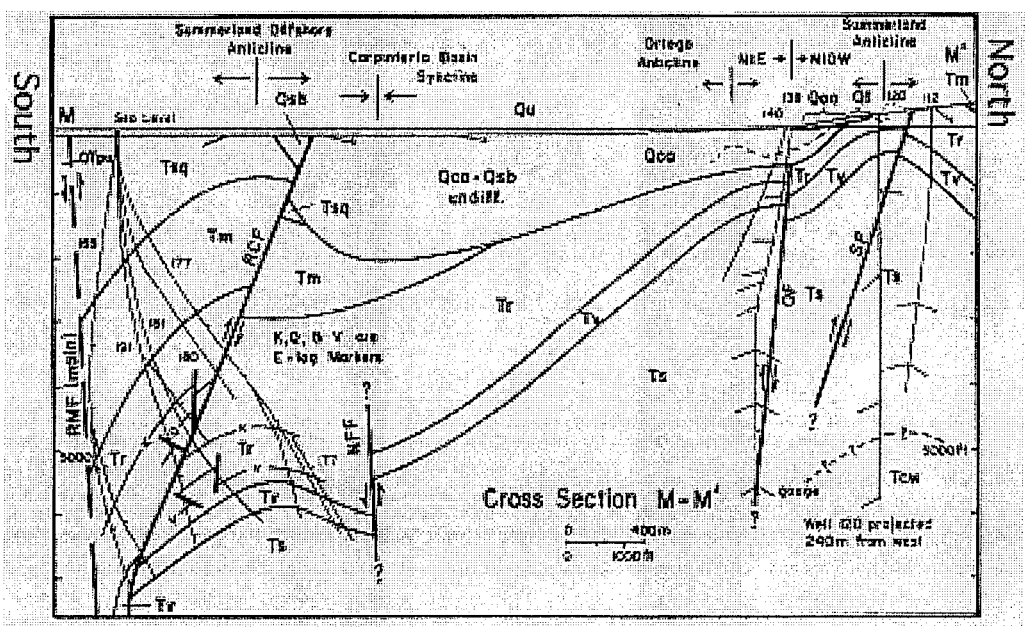

Figure 3. Geologic north-south cross section, MM', through Summerland. SF is the Summerland Fault, and OF is Ortega Fault. Upper marine layers are Casitas formation (Qca) and alluvial (Qoa). Deeper layers offshore Summerland are Rincon formation (Tr) and Vaqueros formation (Tv). From *Jackson and Yeats* (1982; Figure 15).

2. BACKGROUND

2.1 Geological Setting

> "The Summerland offshore oil field is located in the Carpinteria Basin, which is a narrow Pleistocene trough along the northeastern coast of the Santa Barbara Channel between the Santa Ynez Mountains and the Ventura Basin. . . . The shape of the Carpinteria basin is defined by the unconformity at the base of Pleistocene horizon. Near Summerland, the Ortega Anticline was folded after deposition of the Casitas Formation, with a NW-SE trend." (*Jackson and Yeats*, 1982) – see Fig. 2.

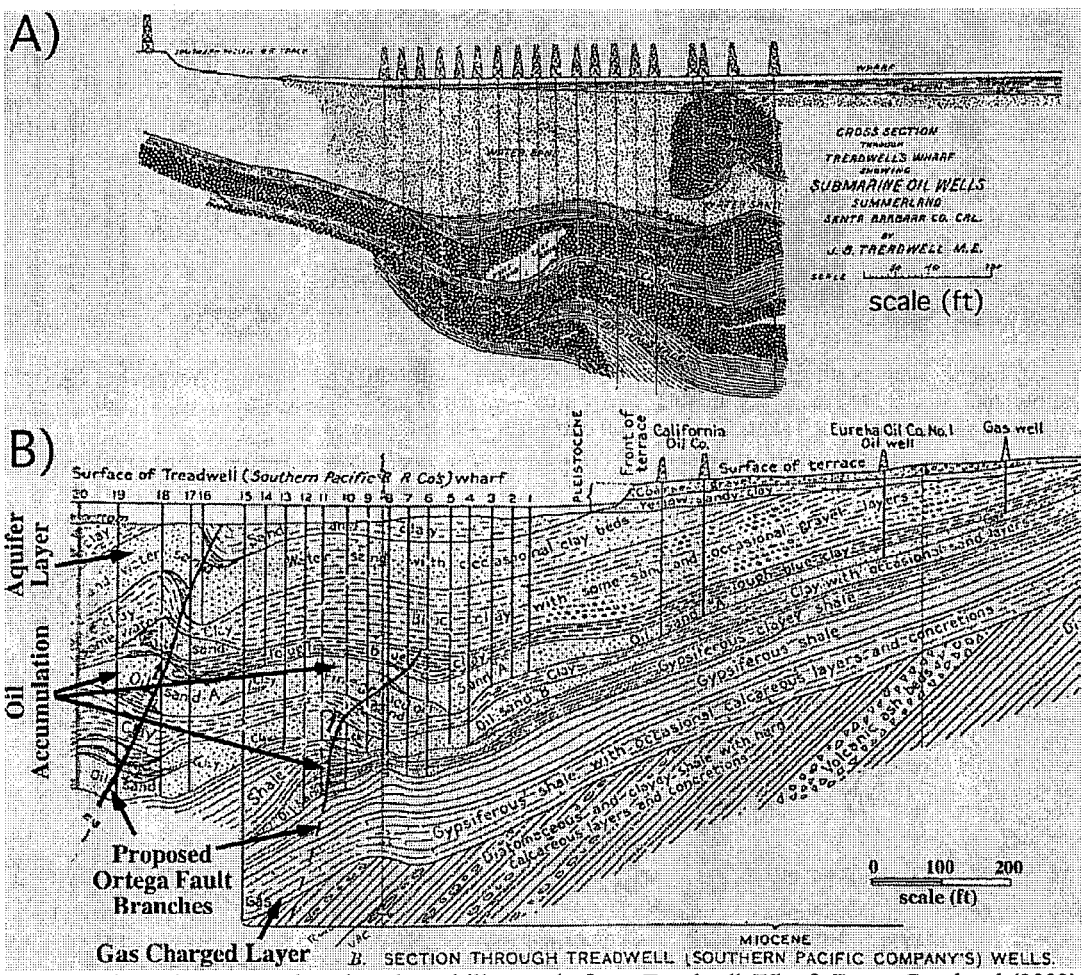

Figure 4. North-south cross sections based on drill records from Treadwell Wharf. From *Grosbard* (2002). We propose the identified faults are branches of the Ortega Fault. Other features are noted on figure by arrows. Scales on panels are in feet.

Slightly inshore of the Ortega Anticline lies the Ortega Fault, which has a slight offshore dip (Fig. 3). A geologic cross section based on the wells drilled from the Treadwell Wharf shows two faults crossing the Treadwell Wharf, which we propose are branches of the Ortega Fault. The inshore branch of the fault is shown crossing the T-10 Well at a depth of ~70 m. The T-10 Well is shown at a distance of ~122 m

offshore (400 ft) (Fig. 4). Further offshore, four different wells (T-16 to T-19) penetrate the offshore branch of the fault where the thickest oil deposits were found. The downward curving fold of rock layers that dip towards the center of the syncline fault allowed accumulation of oil in the more permeable - sand layers. The oil-gas sand layer trended generally shallower towards shore and is shown reaching the surface ~100 m onshore. Outside the fault zone, the oil-sand layer was only a few meters thick. Below the oil sands were gas-charged sand layers. Also noted are sand layers, which could connect to terrestrial aquifers. In fact, one sand layer was noted as having water and surfaced at the location of Wells numbers 17 and 18 on the Treadwell Wharf.

2.2 Historical Background

2.2.1 Wildcat oil exploitation at Summerland

Natural seepage has occurred in Santa Barbara Channel for centuries and probably much longer. For example, indigenous peoples used tar from beach seeps for waterproofing boats (*Hodgson*, 1987). Also, early explorers used the presence of floating oil to indicate proximity to certain areas of the central California coastline. Onshore, nearshore, and offshore oil seeps have attracted prospectors since the late 1800s (*Grosbard*, 2002). Oil production in areas of nearshore marine seepage became feasible through construction of piers and platforms and the placement of casings through the sediment overburden and soft caprock. "The world's first offshore oil was produced in Summerland oil field by wells drilled from piers extending into the Santa Barbara Channel" (*Giallonardo and Koller*, 1978), in an area of natural gas seepage (*Grosbard*, 2002). John B. Treadwell, a mining engineer with the Southern Pacific Railroad, developed a plan to allow train locomotives to use petroleum rather than coal for fuel, with fueling to come from a wharf constructed at Summerland. The wharf could accept fuel shipments and serve as a platform for oil well drilling and exploitation. Located near the train line, the Treadwell Wharf would allow easy refueling at a train stop in Summerland (*Grosbard*, personal communication, 2006). The Treadwell Wharf was 23 m (75 ft) wide and eventually reached a length of 375 m (1230 ft). In 1900, there were 19 wells on the Treadwell Wharf, drilled to depths ranging from 46 to 183 m (150 to 600 ft).

Following construction of the Treadwell Wharf, numerous wharves and oil wells sprouted from the shoreline of Summerland (Fig. 5), exploiting the shallow petroleum deposits. The deposits were found to range from 30 to 120 m deep (Fig. 3). Shortly thereafter (around 1906) the Summerland Field became largely depleted and most production ceased. Total production was 1.37 million barrels from 1895 to 1906. Amazingly, over 412 oil-wells were drilled in the Summerland area (*Arnold*, 1907) with 220 located on the beach and in nearshore waters. A particularly strong winter storm in 1903 removed many wells, a large number of which were inactive. By 1938, only the Treadwell Wharf remained, with production ceasing in 1939, bringing to a close the saga of wildcat oil prospecting and production in the Summerland area. But the Summerland saga did not end with the cessation of oil production.

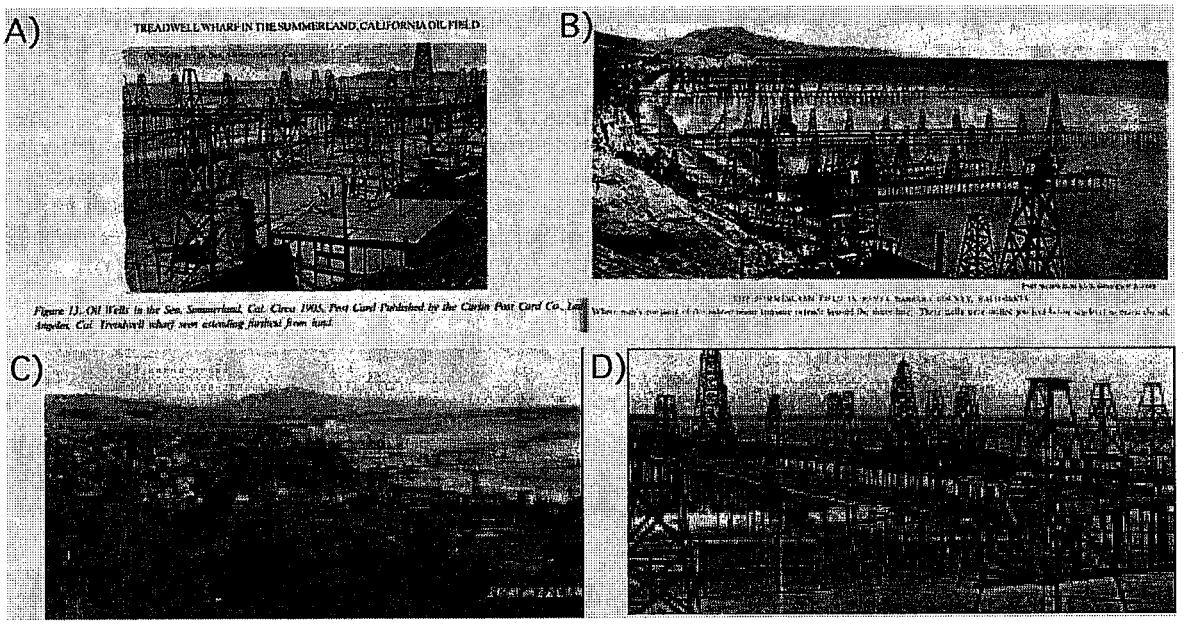

Figure 5. A) and **B)** Postcards photos from around 1900 of oil piers at Summerland (National Geographic, 1920). **C)** Photo of Summerland after a few oil wharfs had been built, and **D)** Beachside detail.

2.2.2 Oil well abandonment at Summerland

The abandonment procedures for depleted oil wells in the early 1900s were primitive, at best. For example, depleted oil wells at Summerland were often stuffed with "... rags, rocks, earth and wooden poles ... (*Fairweather Pacific*, 2000)." A May 1960 survey located ~80 of these wells (*Lindbergh*, 1961). In Dec. 1968, 60 wells were located, their casings cut off, plugged, and capped as a part of the "Summerland Beach Cleanup Project" to alleviate chronic seepage from improperly abandoned oil wells. Typically, modern abandonment consists of excavating and then cutting the well casing pipe at a depth below the level of the unconsolidated sediment. Then, a large diameter steel culvert pipe, one to two meters in diameter, is placed over the cut-off well pipe and filled with concrete, creating a 'cap.'

Since then, it was reported several times that the abandoned Treadwell-10 Well (T-10 Well) and/or the surrounding seabed, located offshore Summerland in 5.2 m of water, continued seeping (*Freckman*, 1981). Replugging and capping of some wells occurred in 1975 (*Lammers*, 1975) and again, when "three historic wells were abandoned by plugging and capping with cement in 1993 using state of the art techniques. These wells included what was believed to be the T-10 Well." (*Curran*, 1995).

Despite these efforts, oil and gas from the 'depleted' reservoir offshore Summerland continues to migrate upwards to the seabed through fractures primarily along faults in the overlying layers (natural seepage) and also along low resistance pathways associated with abandoned oil wells (*Fairweather Pacific*, 2000). Today, oil sheens are periodically observed in nearshore waters off Summerland (*Fairweather Pacific*, 2000) and oil mousse is occasionally observed on the west end of Summerland in the vicinity of Lookout Park.

Mapping and magnetometer surveys conducted in nearshore areas in 1994 found 43 sites potentially associated with abandoned oil facilities and/or natural seeps (*PENCO*, 1995; *Golder Assoc.*, 1995). In the 1994 studies, divers found sites with natural oil and/or gas seepage and/or contaminated sediments, and other sites with debris related to oil production, including well casings, some of which were leaking gas

and/or oil and some of which were not. Although previous reports identified the T-10 Well Site as the dominant source of offshore emissions; at various times in recent decades, reports of petroleum leakage from the T-10 Site have differed greatly (*PENCO*, 1995; *Fairweather Pacific*, 2000). Results from our study indicate that this is due to variability in emissions and other natural and observational factors. For most of our study period, spanning 2000 to 2005, the T-10 Well Site was the dominant offshore oil source; although for a part of the study period when the T-10 Well Site was inactive, a nearby site was the dominant source, named in this study the 'S-3' Site.

Also, there have been reports of oil emissions from the intertidal zone. The first estimate, reported by the U.S. Coast Guard (USCG) in 1994, was ~80 liters day^{-1} (0.5 barrel day^{-1}) from the vicinity of Becker Onshore, located in the intertidal area of the Summerland beach below the west end of Lookout Park. A more recent estimate in July 2003 as part of this study at the same site was 12 liters day^{-1} through a sand overburden that was more than 70-cm thick (based on pushing a brass rod into the sand). Seepage from the onshore site is only grossly apparent at minus tides and when the sand overburden is minimal. Because, for much of the year, minus tides don't occur during daylight hours and the sand overburden during the study was generally very thick, on-shore oil emissions seldom were observed.

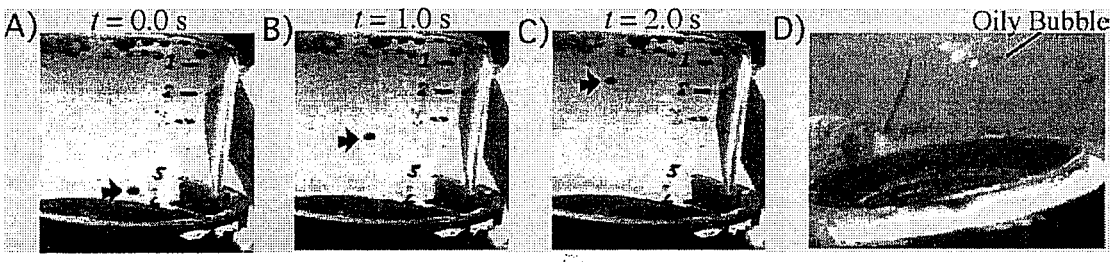

Figure 6. A)-C) Image sequence of a black (very oily) bubble and **D)** three clear (non-oily) bubbles.

3. STUDY APPROACH

3.1 Surveys and Mapping

Surveys were conducted on the beach, sea surface, and at the seabed nearby the T-10 Well Site by SCUBA divers. Beach surveys were conducted by the California State Lands Commission (CSLC), United States Coast Guard (USCG), and Department of Fish and Game - Office of Spill Prevention and Response (DFG-OSPR) from 9/2002 to 4/2004 to locate, describe, and quantify beach oil, and record observations of wildlife oiling. A total of 51 beach-surveys were conducted over the 19-month study.

3.1.1 Sea-surface surveys and seepage trends

Sea-surface surveys were conducted using global positioning systems (GPS) from small boats to identify seepage trends. A seepage trend is where locations of seepage are oriented in a general direction - although the seepage trend need not be straight and can include curves or be jagged. Further, typically seepage trends are discontinuous, but cannot bifurcate. In the Coal Oil Point seep field, a few kilometers to the west, seepage trends have been related to subsurface geologic structures including faults (*Hornafius et al.*, 1999). GPS locations were recorded where both non-oily bubbles (termed clear bubbles) and very oily bubbles (termed black bubbles, which appeared as solid oil droplets), were surfacing. Hereafter, non-oily bubbles will be termed clear bubbles (Fig. 6A) and very oily bubbles will be termed black bubbles (Fig. 6B). Because black bubbles, located immediately below the air-water interface, can persist for significant time before bursting, up to order 100

seconds, they may have drifted a significant distance from their original surfacing location depending upon current velocities. Thus, the locations of floating black bubbles at the sea surface were not recorded, although their presence and the direction of the currents helped guide surveyors toward likely seep locations. Also guiding surveys were seepage trends from previous surface surveys and predicted locations of subsurface faults based on shoreline features. Furthermore, where black bubbles and clear bubbles escaped from the same vent, such as observed at the T-10 Well Site and other Summerland sites, black bubbles rose to the sea surface at a significantly slower rate (about an order of magnitude slower) than clear bubbles and surfaced some distance downcurrent of the clear bubble surfacing location. Clear bubbles tended to surface almost directly over the seabed emission vent location and burst almost immediately (generally, much less than a second). Thus, it was found that clear bubbles provided a better estimate of seep locations on the seabed and typically could be related to the surfacing of black bubbles downcurrent.

3.1.2 Seabed sediment surveys

Seabed sediment-surveys were conducted by SCUBA divers at several sites, including the Treadwell T-10 Well Site. These surveys located structures on the seabed and mapped the subsurface distribution of gas and oil emissions near the T-10 Well Site and a second oil emission site, termed the S-3 Site. In these surveys, divers inserted brass probes, notched at 10 cm intervals, into the sediment at set distances and angles from the T-10 Well Site. The total penetration depth, depth of oiling, and depth at which gas (if any) appeared were recorded.

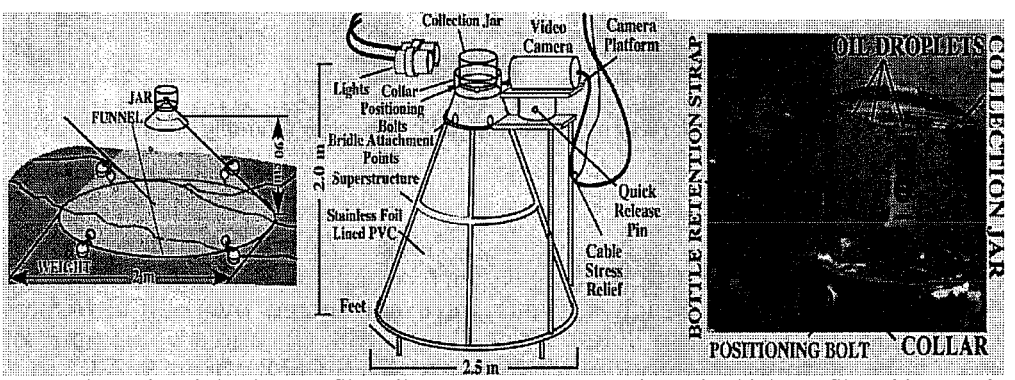

Figure 7. A) Schematic of the low-profile, oil-capture seep-tent, and **B)** the high profile, video-monitored oil-capture seep tent. **C)** Image of black bubbles entering collection jar on the high profile seep-tent.

3.2. Seep emission quantification

Seep tents of three different designs (Figs. 7 and 8) were deployed in separate operations in nearshore waters off Summerland to quantify oil and gas emissions, and are described below.

3.2.1 Low-profile seep tent

The low-profile seep tent was a modification of a turbine seep-tent and was deployed to collect oil and gas. The low-profile seep tent was the base of a turbine seep-tent without the turbine (*Leifer and Boles*, 2005b). This tent funneled bubbles into a sample collection jar (Fig. 7A). The tent was a 1-m tall cone with a 2-m base diameter constructed from 0.16-mm (1/16-in) thick sheets of polyvinyl chloride (PVC) plastic, pop riveted together. The cone was riveted to a support frame of 1.2-cm (1/2-in) diameter PVC pipes. The bottom of the support frame was a PVC pipe ring that was attached to the tent plastic by a rope threaded through a series of holes at

the tent's bottom edge. A deployment bridle was attached to three eyebolts in the bottom ring. This configuration evenly distributed stress during recovery, when the tent acted like a sea anchor. Five 2-kg diving weights were connected to the ring to keep the tent on the seabed despite sea surge and current. A stainless steel funnel was inserted into the apex of the low profile tent to direct oil and gas into the inverted glass sample jar. The jar was filled with seawater and was secured to the funnel and frame by a quick release strap. Divers periodically retrieved, capped, and replaced the jar with new ones to facilitate quantification efforts and to minimize the likelihood of spillage.

3.2.2 High-profile seep tent

A high-profile oil-capture seep-tent area (2.5-m diameter and 2-m tall) was designed and constructed (see Fig. 7B). The tent's steeper profile helped to reduce the adherence of oil to the tents inner surface and its wider mouth increased the collection area. The tent was constructed from 0.16-mm (1/16-in) thick PVC sheeting, pop riveted together. Its interior surface was lined with aluminum foil glued to the PVC funnel with contact cement. The tent had a 2.5-cm (1-in) diameter PVC-pipe framework, which provided support and attachments for stability weights, bridle hook-ups, video camera, and feet. The feet were installed to hold the tent above the seabed, reducing the tendency of swell and tent movements to disturb and release oil from oil-saturated sediment below the tent's edge. Holes drilled into the PVC pipe framework to allow water to enter during deployment, thus reducing overall buoyancy of the tent.

A clear, 200-ml, wide mouth glass collection jar was inverted and mounted over the cone's narrow end and collected gas and oil (Fig. 7C). The jar sat on the rim of a cut stainless-steel funnel mounted in the tent's apex. The cutoff funnel opening was several millimeters narrower than the jar opening. Modifications to the cone tent for the 2005 deployments are described below.

Jars were numbered and marked every 1 cm for a video size-scale. A video camera (SuperCam 6500, DeepSea Power and Light, San Diego, CA) transmitted images of the jar to a shipboard video recorder. The camera was mounted on a plate with an attached PVC pipe that was tightly inserted into a larger PVC pipe mounted on a platform secured to the tent framework. A quick release pin secured the camera to the mount. Two 300-Watt undersea, AC powered lights (DeepSea Power and Light, San Diego, CA) backlit the jar and its contents, overpowering the ambient light and providing sufficient illumination to use a sufficiently fast shutter speed to prevent blurring of clear bubbles. It is important for bubbles to be backlit for identification because top illuminated (ambient), bubbles appear as half-moons, while backlit bubbles appear as continuous convex outlines–i.e., no concave portions (*Leifer and MacDonald*, 2003). Concave portions lead to erroneous bubble sizing. The lights also allowed nighttime operation. The video camera was remotely controllable, thereby allowing selection of a sufficiently fast shutter speed to prevent motion blurring (*Leifer et al.*, 2003).

The high profile seep tent was successfully deployed at the S-3 Site in ~6-m water. However this high profile tent proved unsuccessful in the shallower water at then Treadwell T-10 Well Site due to its large cross-sectional area, the uneven seabed, the projecting caisson edge, and the strong surge from swell.

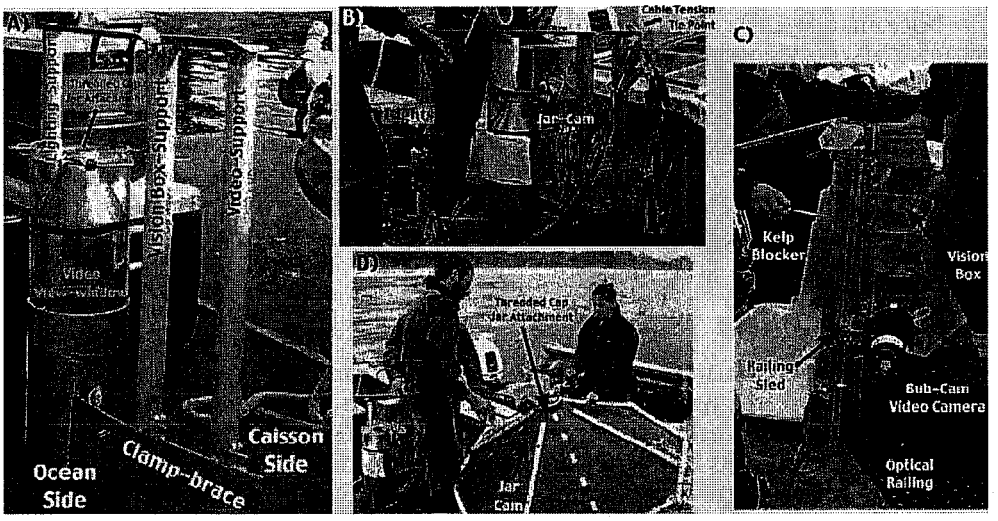

Figure 8. Oil and gas capture seep tents – **A) –C)** Minimal-profile, tube oil-capture seep "tube tent," and **D)** Stainless-steel lined, low-profile "cone tent." Tent components noted on figure.

3.2.3 Minimal-profile, "tube-tent" seep tent

To reduce the effects of swell induced surge on the oil collection tent, a "tube-tent" was designed and developed specifically for use at the T-10 Well Site (Fig. 8). This minimal-profile tent consisted of a clear acrylic vertical tube, supported by a welded aluminum framework that was designed to be clamped to the southeastern edge of the T-10 Well caisson. A stainless-steel funnel was mounted inside the 20-cm diameter acrylic tube and directed gas and oil into a collection bottle. A threaded cap with a large central hole was epoxied into a support ring atop the funnel, and collection jars were threaded into this cap. This eliminated the need for a restraining strap as used in a previous deployment (*Leifer et al.*, 2005), which had interfered occasionally with the video imaging in previous deployments. The acrylic tube was notched at its base to fit over the edge of the caisson, and the entire acrylic tube was slid into an aluminum tube, slightly higher than the exposed portion of the caisson wall. This aluminum tube was cut so that it would fit over the edge of the caisson to provide strong support for the base of the acrylic tube. Oil and gas seepage arose from vents located in a small region (~5-cm diameter), on the interior on the inside of the caisson near its weld seam, thus the notch (and tube) was off-center, protruding only ~3 cm outside the caisson's wall. Although the interior of the tube tent was flush with the accumulated sand and gravel and the exposed concrete plug interior to the caisson, exterior, it was several centimeters above the seabed. To prevent surge from penetrating the tube tent, packing foam was inserted into this gap. The height of the aluminum tube that stabilized the base portion of the acrylic tube was lower than the base of the stainless steel funnel. This provided a clear window for video observation of bubbles. A translucent white screen was secured to the exterior of the acrylic tube at this height, on one side of the tube, to provide a back illumination screen.

The aluminum tube was welded to a plate of 0.318-cm (1/8 in) thick aluminum sheet, cut to the exterior profile and bent to match the 1.75-m (5 ft 9 in) arc of curvature of the caisson wall. The 5 ft 9 in diameter was measured by scuba divers. This aluminum band was clamped to the caisson wall at four points. Three vertical 5.1-cm (2 in) diameter aluminum tubes were welded to the support sheet. These

aluminum tubes extended to slightly above the height of the acrylic tube and had lugs welded at their upper extent. Finally, bolts connected an aluminum top-plate to the tubes and provided greater stability. Eyebolts in the top plate also were connected to stabilization lines, which were attached to weights located a few meters to either side of the tube-tent. The video camera, lights, and vision box were mounted by moveable sleds on optical railing supported by vertical aluminum poles. The vision box is described below. The optical railing was secured to the vertical poles with hose clamps, and allowed the video equipment to be repositioned and locked in place. The video camera and lights were the same as described for the high-profile tent. Because underwater visibility offshore Summerland could be as little as a few centimeters, a detritus free path was needed between the camera and the measurement volume. To create such a path, we constructed and installed a 'vision box.' This was a clear acrylic box that was filled with fresh water through a hole sealed with a rubber stopper. The vision box was positioned almost flush with the front of the video camera. Because the vision box was filled with clean water, it did not need to be watertight and was close to neutrally buoyant. The 30-cm distance allowed a zoom setting that decreased parallax uncertainty. Parallax error is an optical phenomenon whereby a closer object appears larger than a more distant object of the same size. Parallax errors increase with decreasing lens focal length - i.e., wide-angle zoom settings. Had the video camera been mounted flush with the acrylic tube, a very wide-angle zoom setting would have been required, which would have resulted in large parallax uncertainties. A thick piece of rubber (0.5-cm thick sheeting) was mounted on the side of the vision box at both ends and protruded slightly to prevent abrasion damage between the vision box, camera, and tube tent.

Finally, a large plastic box was cut so that it could be mounted over the center portion of the tube tent including the camera, acrylic tube, vision box, lights and screens (Fig. 8C). This plastic box blocked kelp from becoming trapped in the path of view of the camera, and the lights.

3.2.4 Modified low profile "cone-tent" seep tent

For the 2005 deployments, the interior of a low-profile, PVC-plastic walled, *cone-tent* (Fig. 8D) was covered with 0.05 mm thick stainless-steel foil. This allowed the interior of the tent to be rinsed with dichloromethane (DCM) solvent to remove adhered oil without dissolving the plastic walls of the cone tent. Stainless-steel foil was used because of its greater strength compared to aluminum foil used during a previous deployment. The stainless-steel foil was secured to the tent interior by a combination of stainless-steel rivets and stainless-steel adhesive tape. Collection jars were mounted onto the modified cone tent using a collar and threaded cap similar to those on the tube tent - a threaded cap with a large central hole was siliconed into a collar epoxied to the apex of the tent. The cone-tent also was fitted with a small "fish finder" video camera mounted on a spar. The video camera monitored the jar and had a very wide field-of-view that allowed everything to be in focus.

3.2.5 Sample protocol

Collection jars were retrieved periodically for later analysis, with the deployment and retrieval times recorded. Oil samples were collected in EPA-certified clean glass containers with Teflon lids, and stored in a cooler with ice onboard the boat. To preserve gas, each lid was wrapped in self-annealing tape. Each bottle lid was wrapped in self-annealing tape. In three cases, bottles leaked oil into the cooler due to outgassing and overpressurization Further, prior to shipping, each jar was wrapped in aluminum foil, placed in a Ziploc™ bag, and then bubble wrapped. Thus, if breakage occurred during shipping, the oil could be recovered for the jar. After

recovery of the tent, the interiors of both tents were rinsed with DCM into sample jars. Samples were shipped in a cooler with ice to Texas A&M Geochemical and Environmental Research Group (GERG) for analysis by Steve Sweet. Gas volume in each jar was determined by first weighing the jar, then carefully filling the jar with distilled water to the upper edge and then re-weighing to determine the water volume, which is equivalent to the gas volume. A known portion of the oil content was removed to a separatory funnel and the oil extracted by dichloromethane until the organic layer was clear. A known volume of the extract was weighed using a Cahn electrobalance.

3.2.6 Petrolarium

Beach emissions were quantified at the Becker Intertidal Seep, located on the beach below the west end of Lookout Park, using a custom constructed device we termed a "petrolarium." This was a bottomless and topless glass tank (30-cm square) that was placed around the emission site on the sandy beach just before nadir of the lowest low of a minus tide (Fig. 9). A 6-cm (2.5 in) diameter tube was placed over the main vent, and allowed to fill with oil to a depth of ~1 cm, after which it was emptied with a 25-ml syringe. Collected oil was then deposited in 238-ml (8-ounce) jars. The cylinder was not allowed to fill to a depth greater than 1 cm because of concern that the greater hydrostatic pressure would decrease oil emission rates. Collection continued from 14:46:00 until 17:05:42 hours (PST), after which the amount of oil accumulated in the petrolarium, outside the central cylinder, was collected and estimated.

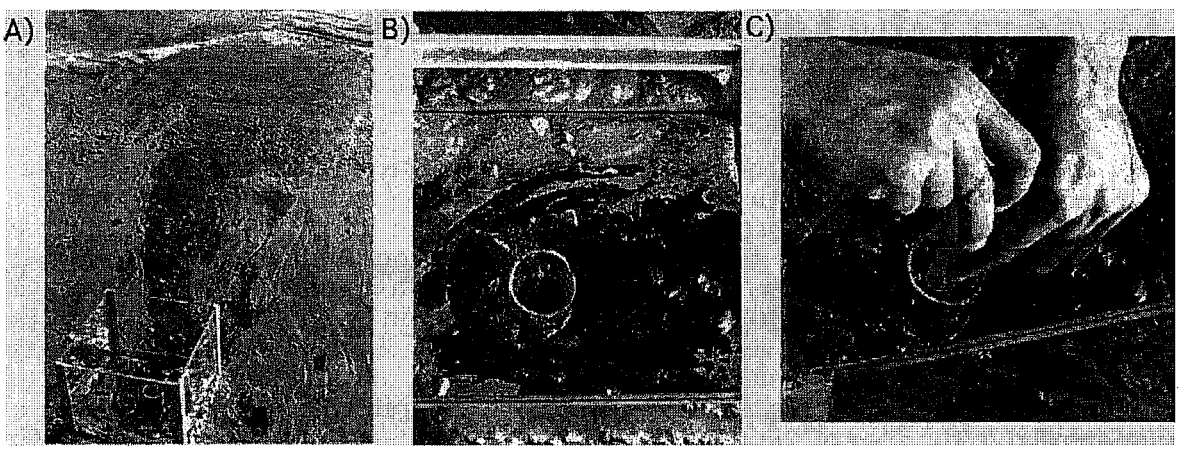

Figure 9. Images of the petrolarium. **A)** The petrolarium when first emplaced. **B)** Oil and gas bubbled up in the central tube and **C)** was continuously removed with a syringe. Collected oil from was deposited in bottles.

Figure 10. Aerial image of the approximate location of the Treadwell Wharf (dashed lines), showing sheens from the T-10 Well Site, and two other oil emission sites, S-4 and S-5. View is northeast looking, Also shown is the approximate location of the S-3 Site. The S-1 and S-2 Sites are out of the field of view. The UCSB boat is a 7-m (21 ft) Boston Whaler.

4. OIL AND GAS EMISSION OBSERVATIONS

4.1 Seabed emission observations, 2003

In the Summerland area, numerous seepage areas create oil sheens and occasionally, contributed to beach oiling. Sea surface and aerial survey images (Fig. 10) were used to guide seabed surveys along with GPS coordinates provided by the California State Lands Commission (CSLC).

4.1.1 Location and identification of primary oil emission site, 2003

On 5 and 6 February 2003, SCUBA divers found a 1.2-m diameter, concrete filled metal caisson cap, which had a hard asphaltic plug protruding from the interior wall. Initially this structure was proposed to be the cap of the T-10 Well, because it was found at the CSLC provided T-10 Well coordinates. However, due to differences in its diameter from the 1975 description of the T-10 Well (*Fairweather Pacific*, 2000), and the water depth, the site was termed the S-3 Site pending further confirmation of its identity. Subsequently, the S-3 Site was determined to be ~20 m to the west and to the southwest of the actual Treadwell T-10 Well and further offshore in deeper water. The location of the S-3 Site was thought to be in the vicinity of the historic Moore Pier - its smaller diameter suggested the S-3 Site was not the T-10 Well Site. Although fresh oil was neither escaping from the structure nor from the seabed within 10 m of the cap; the hard asphaltic plug appeared to have originated from an oil source within the caisson. The asphaltic plug was formed from oil, which had leaked from the seam between the concrete plug and the caisson metal sometime in the past. This plug was not noted during surveys in 1994 or 2000 when the area surrounding the purported T-10 Well was leaking.

On 20 May 2003, the cone tent (Fig. 7A) was deployed at the S-3 Site at a depth of ~5.2 m on a flat sandy seabed with a sand overburden of undetermined thickness, in nearshore waters off Summerland, CA. Field deployments were scheduled for periods of negative tides. Divers noted droplets and stringers of oil and gas bubbles emerging from holes in the sandy bottom, and surface slicks originated from the region. The tents were deployed for 20 minutes. The gas to oil ratio was estimated at 100 to 1 (analysis by the OSPR's Petroleum Chemistry Laboratory) with a total estimated oil

seepage of ~36 ml day^{-1} for the entire area surrounding the tent. Uncertainty in the oil-gas seepage estimate arose from uncertainty in the total area of seepage at the seabed from which oil was not collected.

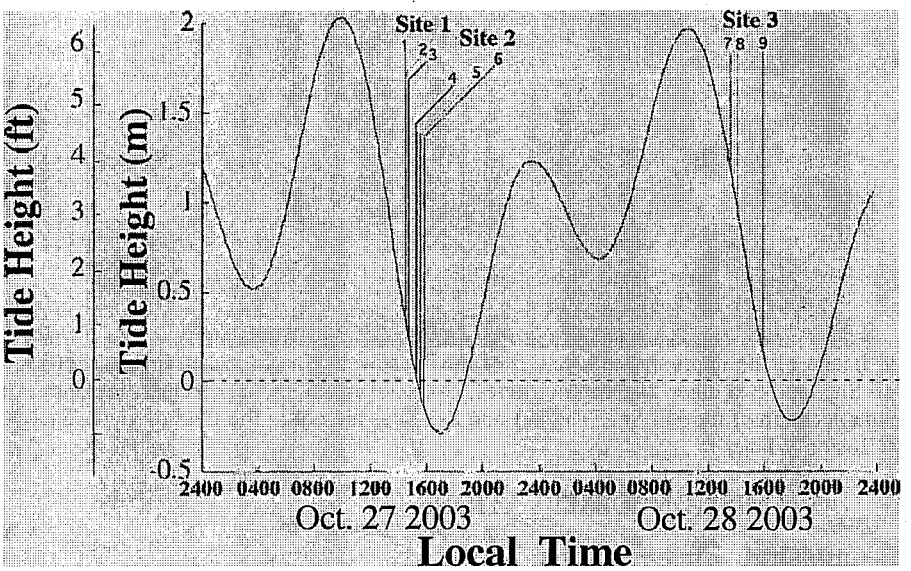

Figure 11. Tide height for 27-28 Oct. 2003. Times of samples 1 through 9 noted on figure. Tide heights from USC tide predictor (http://tbone.biol.sc.edu/tide/).

4.1.2 Oil and gas emission measurements at sites S1-S3

On 27-28 Oct. 2003, divers positioned the cone tent (Fig. 7A) at three seepage areas, termed S-1, S-2, and S-3. Deployments coincided with significant minus tides, although samples were not collected at the nadir of the lowest low tide as safety considerations required retrieval of equipment at dusk. The measurements are summarized in Table 1. The S-1 Site was located on featureless sandy bottom, similar to the deployment site of May 20, 2003. Seep bubbles appeared clear and the measured gas to oil ratio was 111,000±55,000 to 1. Gas seepage was estimated to be 90.4± 14 L day^{-1} for the area covered by the tent. The oil emission rate was estimated to be 0.98 ml day^{-1} for the area covered by the tents. Bubbles at the S-2 Site were similar in appearance to the S-1 Site as was the gas to oil ratio of 94,000 ± 20,000 to 1. At both sites, only clear bubbles were emitted. Estimated daily oil and gas seepage rates for the area covered by the tents were 1.07 ± 0.4 ml day^{-1} of oil and 96.2 ± 21 L day^{-1} of gas, respectively.

The S-3 Site was located at 34° 25.0375'N, 119° 36.019' W ~20-m southwest of the CSLC coordinates for the T-10 Well. Note, the location of the S-3 Site was reported in *Leifer et al.* (2004) at 34.4180579°N, 119.5984375 in NAD27, or 34°25.038'N, 119°35.906'W in NAD83. The discrepancy arose from mistaken understanding of the coordinate system of the site location, NAD27 versus NAD83.

At the seabed, the S-3 Site was sand and cobble, subcanopy forming algae, and the ornate tubeworm, *Diopatra ornata*. A partially buried concrete cap and metal form were found. At the S-3 Site most seep bubbles were black. Seepage at this site was the most significant source of sea surface oil sheens during our October 2003 survey and had a measured gas to oil ratio of 8.36 ± 6.9 to 1. Gas seepage was 350±330 ml day^{-1}, oil seepage was 51.5 ± 65.5 ml day^{-1}. Based on the sea surface area where oily bubbles

were surfacing, it was estimated that 10% of the seabed was covered – i.e., for the S-3 Site, around 500 ml oil per day might be emitted. The large variability arose from an increase by an order of magnitude in both oil and gas emissions for the last of the three samples collected at the S-3 Site (Table 1), which likely was due to the decreasing tide.

Table 1. Results of analysis of collected sample jars for oil and gas. Coordinates in NAD83.

Sample	Time deploy	Time (min)	Oil (ml)	Oil Flux (ml day^{-1})	Gas (ml)	Gas Flux (L day^{-1})	Gas/Oil ratio
Site S-1		**27 Oct. 2003**		**34°25.0548'N, 119°35.878'W**			
1	14:35	5.15	0.0027	0.75	364.60	101.95	135,000
2	14:39	6.20	0.0027	0.63	407.70	94.69	151,000
3	14:46	5.00	0.0054	1.56	259.40	74.71	48,000
Site S-2		**27 Oct. 2003**		**34°25.0687'N, 119°35.922'W**			
4	15:25	6.32	0.0027	0.62	318.50	72.57	117,000
5	15:36	4.08	0.0036	1.27	298.70	105.42	83,000
6	15:52	3.46	0.0032	1.33	265.30	110.41	82,900
Site S-3		**28 Oct. 2003**		**34°25.0375°N, 119°36.019'W**			
71	3:34	31.3	0.4910	22.6	8.00	0.368	16.3
81	4:05	112.29	0.4310	5.53	1.50	0.019	3.48
91	5:56	26.60	2.3360	126.46	12.40	0.67	5.31

Mean Site Values	Oil Flux (ml day^{-1})	Gas Flux (L day^{-1})
S-1 Site	0.979±0.4	90.4±14
S-2 Site	1.072±0.4	96.2±20
S-3 Site	51.5±65.5	0.35±0.33

4.1.3 Oily bubble video analysis

Video was collected during the tent deployment at Site S-3 and analyzed. The analysis techniques are published in *Leifer et al.* (2004), and are presented in Appendix 1. Analysis of oil droplet video provided time series (0.033 second resolution) of petroleum emission, which allowed estimation of the oil and gas transported by each oily bubble. In brief, video was digitized into a series of frames, which, after some image processing, were thresholded and bubbles sized. By tracking bubbles through the frame sequence, the bubble rise velocities were determined.

Bubble size and velocity distributions, Φ, were calculated by the method of *Leifer and Boles* (2005a), where size distribution is expressed as $\Phi(r)=Ar^S$, where r is the equivalent spherical radius, S is the power law exponent, and A is a constant. Rise velocities V_B, were used to infer bubble oiliness based on comparison with laboratory-based parameterizations of bubble V_B absent any oil effects (hydrodynamics or buoyancy). Bubble oiliness was determined by calculating the buoyancy loss required to decrease the predicted V_B (*Leifer and Patro*, 2002) to the measured V_B, assuming the effect of oil was purely on the buoyancy, i.e., no hydrodynamic effects. This is a first step, and the appropriateness of this assumption was tested by comparing the estimated total oil emissions with the analyzed oil captured in the jar.

Since oil is a surface-active substance (surfactant), we assume that bubbles with trace oil (i.e., no oil-induced buoyancy effects) behave like non-oil surfactant-

contaminated bubbles. Surfactants are compounds or particles with both hydrophobic and hydrophilic sites that "prefer" – i.e., they have higher adsorption rates than desorption rates on gas-water interfaces, and are common in the ocean from algae and leptopel (acellular organic detritus). Surfactant-contaminated bubbles are termed 'dirty,' which is defined as hydrodynamically dirty. Dirty bubbles both rise and exchange gas slower than hydrodynamically clean bubbles.

4.1.4 Bubble-emission size-distribution

The bubble emission size-distribution, Φ, (# μm^{-1} s^{-1}–number of bubbles emitted per second per size increment) for these oily bubbles was narrowly peaked at r~1500 μm (Fig. 12A), which is typical for low flow vents where bubbles escape singly or in bubble lines (*Leifer and Boles*, 2005a). The power law exponent, S, was 3.84. Since $S >$ 3, the peak in the bubble volume was close to the peak in Φ. Bubble breakup was not observed for the low emission vents at Summerland. Φ at the seabed should be very similar, although slightly smaller. Bubble sizes at the camera were at most 4.8% larger than at the seabed due to the decrease in hydrostatic pressure.

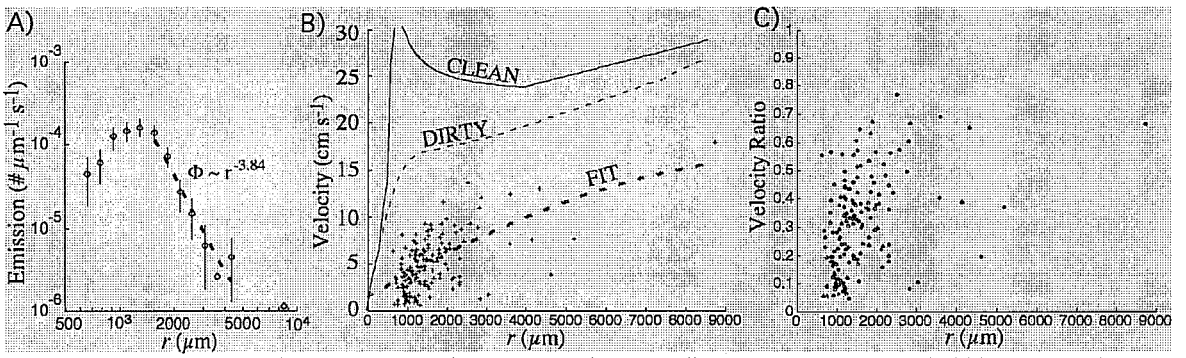

Figure 12A) Bubble emission size-distribution as a function of radius, r, for all analyzed bubbles at the Site S-3. Vertical lines are error. Also shown is the fit to data over r range shown. **B)** Rise velocity versus radius, r, of all black bubbles and fit to data over size range shown. Also shown is the dirty bubble (clear, non-oily, but surfactant contaminated) V_B parameterization in stagnant water from *Leifer and Patro* (2002) and a polynomial, least-squares fit to the data. **C)** Ratio of clean to dirty rise velocity with respect to r.

4.1.5 Black, oily bubble rise velocity

Bubble analysis confirmed that all bubbles were heavily oil contaminated (Fig. 12B), i.e., black bubbles. In particular, V_B was significantly slower than for dirty (non-oily – i.e., clear) bubbles. The fit had a finite velocity (1.29 cm s^{-1}) for a zero radius bubble, indicating the difficulty of forming very small oily bubbles. The ratio $V_B/V_{B-Dirty}$ (Fig. 12C) varied from 4.7% (oilier) to as high as 77% (less oily) with larger bubbles generally having higher velocity ratios, i.e., the least oily. Some small bubbles also had very high velocity ratios (less oily). The mean velocity ratio was 32±17%. The scatter in V_B (r), up to a factor of three (Fig. 12C), suggests variations in oil to gas ratios - the analysis did not show significant non-petroleum detritus, so only hydrocarbons could have reduced the buoyancy.

4.1.6 Video-derived oil emission rate estimate

Using the approach outlined above, the oil and gas emissions were estimated and compared with the measured value (*Leifer et al.*, 2004) to check the assumption that oil only induced buoyancy effects. Since only a 10-minute video sequence (~20,000

frames) was analyzed, this comparison assumes that the emission rate and Φ remained roughly constant over the collection period. See Fig 13 for an example, calculated, time series. Seabed emission time was estimated using the observed V_B for each oily bubble. Total predicted oil emission for Sample 8 from the video analysis was 37-mg oil in 607 s, versus the collected 0.43 ml oil in 6737 s. Therefore, neglecting the effect of oil on bubble hydrodynamics yielded a significant overestimate in bubble oiliness. The seabed emission time series (Fig. 13) was calculated by summing all emissions during each 2 s period and normalizing to an emission rate of 0.43 ml oil in 6737 s. By far, the largest oil emission was a single pulse at ~375 s with two smaller, but significant, pulses at ~125 and ~275 s.

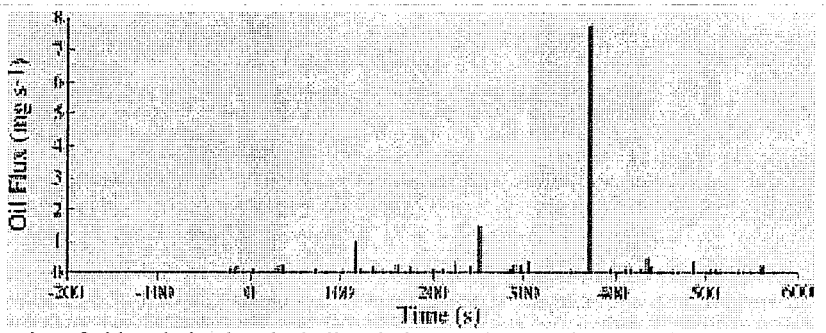

Figure 13. Time series of video-derived seabed oil emissions at the S-3 Site. Zero time is arbitrary.

4.2 Seabed emission observations, 2004

A seabed SCUBA survey of several emission sites was conducted 7 Dec. 2004 in conjunction with an aerial survey. These efforts were in preparation for a planned deployment of the high profile seep tent (Fig. 7B) on 13 Dec. 2004 (Fig. 10).

During the seabed survey, the Treadwell T-10 Well Site (34° 25.087'N, 119° 35.951' W) and oil and gas were observed escaping from an area few centimeters inside the 175-cm diameter concrete/metal cap from the north-northeast wall of the T-10 Well. Seepage was also observed immediately exterior to the caisson from the south-southwest edge. Both emission sites were adjacent to metal seams in the caisson wall. The Treadwell T-10 Well Site was located 110 m northeast from the S-3 Site (Fig. 10).

In October 2003, at the S-3 Site (34°25.0375°N, 119°36.019'W), both black (oily) and clear bubbles were observed escaping from the caisson; however, in October 2004, only gas was observed escaping from the caisson. Although both black and clear bubbles were observed at the sea surface, the source of the black bubbles was not located. There were numerous pipes and other debris on the seabed in this area. Although both the T-10 Well Site and the S-3 Site were active, the T-10 Well Site emitted significantly more oil than the S-3 Site.

A fourth site, the S-4 Site (34° 24.044' N, 119° 35.959' W), was located where oil and gas was escaping from what appeared to be the remains of two metal well casings, 20 to 25 cm (8 to 10 in) in diameter, that protruded into the water column to a height of ~ 3 m (9 ft) above the seabed. Sheens were consistent here. These pipes were very corroded and cracked. Both black bubbles and clear bubbles were observed rising out of their tops. Also, the S-4 Site was marked with a spar buoy. At the sea surface, a few black and clear bubbles surfaced per second. Due to its relative insignificance compared to the T-10 Well Site, quantification of oil and gas emissions were not attempted.

A fifth oil emission site, the S-5 Site, ~10 m south of the S-4 Site, was surveyed at the seabed. Here, black and clear bubbles were observed escaping from a shallow depression. Adjacent to the depression was a rock ridge 10 to 15 cm high, ~2-m long

and ~1-m wide. Again, due to the relative insignificance of emissions, quantifications of oil and gas emissions were not attempted.

On 13 Dec. 2004, deployment of the high profile tent was attempted at the T-10 Well Site in ~3 m of water. Long period swells with ~20 second intervals and ~30 cm in height, created very strong bottom surge, which damaged the tent. As a result, the tent was recovered after just 5 minutes in the water. Consequently no gas/oil collection was done.

4.3 Seabed emission observations, 2005

An intensive two-day effort was mounted to understand better oil and gas emissions from the Treadwell T-10 Well Site (19-20 July 2005). Mission dates were chosen to coincide with extreme low (-1.2 ft) and high tides (+7.4 ft). Because, the *R/V Garibaldi* was unavailable due to engine problems, a reduced mission was conducted using two 7-m (21-ft) boats.

Prior to deployment of the oil collection tents during 2005, reconnaissance and preliminary quantification efforts were undertaken. These included sea surface surveys (15 July 2005), SCUBA surveys of the T-10 Well Site and other active seepage sites (24 June 2005), preliminary oil emission study (15 July 2005), and oil emission studies (20-21 July 2005 and 18-19 Oct. 2005).

These reconnaissance missions found that the dominant source of oil emissions in nearshore waters off Summerland in July 2005 was the T-10 Well Site, which was much more active than the S-3 Site. In contrast, two years prior, in 2003, the S-3 Site was the dominant oil emission site offshore Summerland during field efforts while the T-10 Well Site was inactive. However, T-10 Well Site emissions in July 2005 were significantly greater than the S-3 Site emissions in 2003.

Seabed surveys also were conducted in 2005 in an area of active gas seepage several hundred meters to the east of the T-10 Well Site, in deeper water (~10 m). These seeps did not correspond to any reported seep locations and were further offshore than any oil facilities extended. The seeps were named the Sea Otter seep due to a lack of sea otters in the seep area. The Seep Otter seep consisted of about a dozen active bubble plumes with no apparent oil emissions. A seabed survey suggested that seepage was controlled by a semi-consolidated layer of seashells ~30 cm below the sandy seafloor. This layer apparently trapped gas that leaks slowly through cracks in the semi-consolidated layer. Poking a rod through this shell layer created new active seep vents.

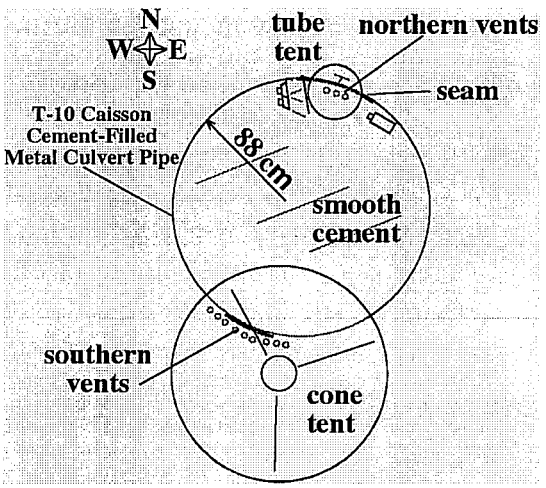

Figure 14. Tent deployment locations at the T-10 Well Site for the 20-21 July 2005 and 18-19 Oct. 2005 surveys. Small circles indicate locations of seepage.

4.3.1 Location of seabed emissions at the T-10 Well Site - July 2005

At the T-10 Well Site, emissions were confined to two areas (Fig. 14). Seepage escaped from a small area ~2 cm interior of the metal wall of the caisson near a seam located on the northeast side of the cap. Seepage also occurred along a span of ~1 m exterior to the south wall of the caisson. SCUBA observations suggested most of the oil emission was from the northeast vents. This visual observation was countered by our quantitative analysis of the collected oil. Visual observations at the seabed and sea surface suggested that oil emissions from the well's southern edge were the greatest.

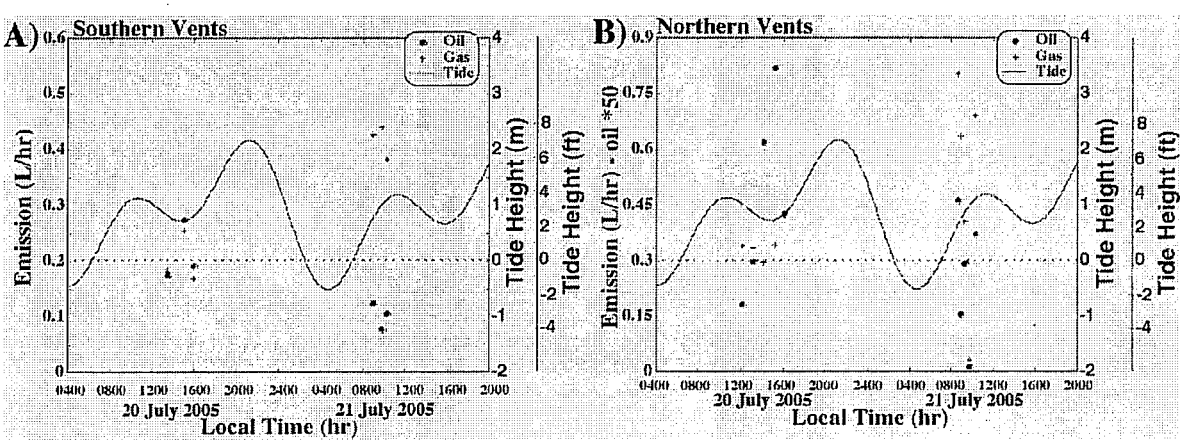

Figure 15. Emissions from the T-10 Well Site for the **A)** Southern vents and **B)** Northern vents and computed tides for July 20-21, 2005. Data key on figure. Tide heights from USC tide predictor (http://tbone.biol.sc.edu/tide/).

4.3.2 T-10 Well Site seabed oil and gas emissions - July 2005

The oil studies were conducted for only a short portion of a tidal cycle because only small boats were available and tent deployment required a few hours. Thus, this study was in part a test of protocols and preliminary effort to quantify oil and gas fluxes. Further, because of the smaller boats, no video monitoring occurred.

An improvement over the 2003 study was that after each deployment, oil that had accumulated on the interior of the tents was rinsed with dichloromethane into a

sample jar. This collected oil was divided among the sample jars proportional to the normalized oil collection. This implies that the oil removed from the tent's inner surface adhered on the tent surface at a rate that was proportional to the emission rate - i.e., a constant fraction of the oil stuck. This can be represented by:

$$E_c(j) = E_T * E(j) / \Sigma E(j) \quad (1)$$

where E is the amount of oil collected in jar, j, E_T is the amount of oil accumulated on the tent's inner surface, and $E_c(j)$ is the corrected amount of oil in jar, j.

July 2005 study results

Tidal heights on the two days (Fig. 15) were comparable; however, the second day sampling was conducted during a rising tide, while the first day was during the higher low tide. For each sample the time used for calculating emissions was the average of the deployment and recovery time.

On 20 July 2005, there was a notable increase in oil emissions at low tide for the southern vents, much greater than indicated on Fig. 15 because the jar on the southern vents was found upon retrieval to have overflowed. Thus, the low tide value (and total emissions estimates) is a lower limit for oil emissions during the deployment. Most of the oil emissions from the T-10 Well Site escaped from the southern vents (note oil emissions from the northern vents in Fig. 15 are multiplied by a factor of 50 for scaling purposes). In contrast, gas emissions for both vents were comparable.

Although the data shows enormous scatter, oil emissions on 21 July 2005 were significantly lower than oil emissions on July 20, 2005. In contrast, gas emissions were higher on 21 July 2005 than 20 July 2005. These differences occurred despite similar tidal heights, although sampling on 21 July 2005 was during a rising tide (+4 ft. tidal level) ~6 hours following a low tide of -1.6 ft at 0446 hours local time. Gas to oil ratios between the northern and southern vents varied significantly, from as high as 1 to 1 for the southern vents tent on 20 July 2005, to as high as 200 to 1 for the northern vents on the second day. For both tents there was an increase in the gas to oil ratio on 21 July 2005 compared to the previous day.

Table 2. Analysis of collected sample jars for oil and gas extrapolated to daily rate for 20-21 July 2005 for the T-10 Well Site.

	Southern vents ($L\ day^{-1}$)	Northern vents ($L\ day^{-1}$)	T-10 Well Site ($L\ day^{-1}$)
Gas	7.4	10.3	17.7
Oil	3.8	0.17	4.0
Ratio*	1.9	60.6	4.4

*volumetric ratio

October 2005 study results

A field effort was mounted 18-19 Oct. 2005 from the *R/V Garibaldi* to monitor oil and gas emissions at the T-10 Well Site through a complete tidal cycle. The decision to collect data through a full tidal cycle was based on data from the marine Coal Oil Point seep field that has shown a tidal influence on both gas (*Boles et al.* 2001) and oil (*Mikolaj et al.* 1973) emissions. At lower tide, the hydrostatic pressure is less, thus it was proposed that a decrease in hydrostatic pressure due to lower tides leads to an increased overpressure in the subsurface fractures. Overpressure (pressure above hydrostatic) is an important process leading to the flow of oil and gas through the

vent system. Thus, an increase in the overpressure leads to greater flow from active vents. Given that significant tidal variations in seepage have been demonstrated for oil and gas elsewhere, it was considered critical to the quantification effort to make measurements through a tidal cycle to develop an empirical model of emissions with respect to tide.

The tube and cone tents were deployed at the T-10 Well Site at the positions shown in Fig. 14. Upon deployment, surface slicks in the vicinity of the T-10 Well Site virtually ceased, indicating that the two tents covered completely the emissions sites on the T-10-Well Site with virtually all the oil and gas being captured. Oil and gas collection jars were retrieved periodically from the tents for later analyses, and the deployment and retrieval times recorded. Water depth was recorded with a conductivity temperature device (CTD, Model SB-39, Seabird, FL), which was attached to a support spar on the topside of the cone tent.

Emission rates for the northern and southern vents of the T-10 Well Site are shown in Fig. 16 versus the measured water depth. CTD data were low-pass filtered with a 60 second block-filter to remove high frequency variations from swell and showed an overall tidal change of 2.3 m (7.5 ft). Gas emission rates were corrected for hydrostatic pressure to standard temperature (20°C) and pressure (STP) - atmospheric, based on the mean water depth and temperature for the deployment time of each jar. A pronounced tidal effect in the oil and gas fluxes due to the decreasing hydrostatic pressure as the tide ebbs is clear in emissions from the seepage areas. Oil emissions rates increased by a factor of ~100 while gas emission rates increased by a factor of ~70. For the northern vents, oil emissions increased by a factor of ~25 and gas emissions by a factor of just ~5 for the same tidal changes. Peak oil emission rates for the southern vents were 4.2 times those of the northern vents, 0.22 L hr^{-1} versus 0.052 L hr^{-1}, respectively. Also, gas to oil ratios were significantly higher for the northern than for the southern vents. Finally, for the southern vents, peak oil emissions occurred ~30 minutes after local low tide, while gas emissions reached a maximum at local low tide. For the northern vents, oil emissions appeared to peak before local low tide, although the oil data were highly variable. Gas emissions, which were even more variable than the oil emissions reached a maximum slightly before local low tide.

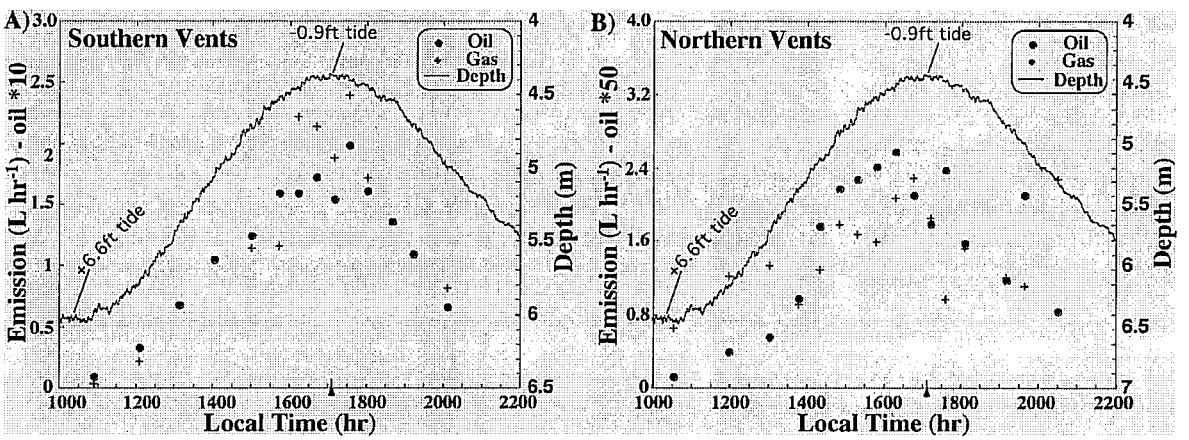

Figure 16. Gas and oil flux rates for the **A)** southern vents and **B)** northern vents of the T-10 Well Site and measured water depth (note reversed depth axis). Note oil emissions are multiplied by factors of 10 and 50 for the southern and northern vents, respectively. Multiplication factors allow the oil and gas emissions to be displayed on the same scale. Gas emissions are corrected to STP. High and low tide times are predicted. Arrow shows local time of low tide. Data key on figure.

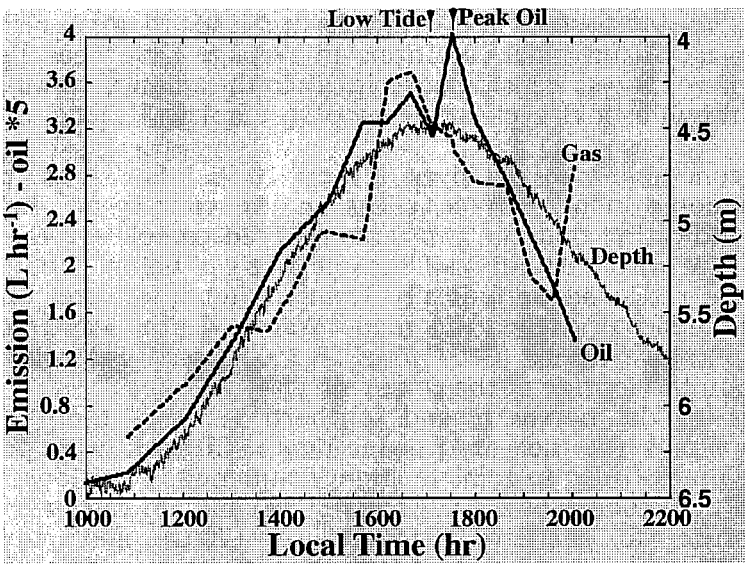

Figure 17. Combined gas and oil emission for the Treadwell T-10 Well Site and water depth with respect to time. Data labeled on figure. Note, oil emissions are multiplied by 5. Arrows shows local time of low tide (measured) and the peak in oil emissions.

Because the jars were deployed and retrieved at different times for the two tents, combining the two emission time series required interpolation. The combined oil emissions, E (L hr^{-1}), from the northern and southern vents (Fig. 17) showed a better relationship to water depth, D (m) and less variability than oil emissions from either southern or northern vents measured individually (Fig. 16). Here D was the CID measured water depth averaged over the deployment time of each jar. This is shown clearly in least-squares, linear-regression analysis fits to the data (Fig. 18). Gas emission rates for the northern and southern vents also closely tracked hydrostatic changes. Also, a delay of ~30 minutes was observed between the local low tide and the time of peak oil emissions.

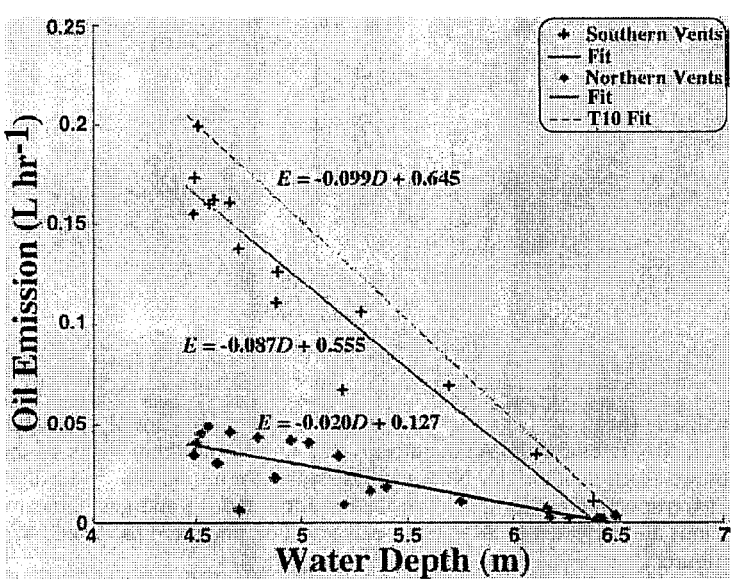

Figure 18. Least squares, linear-regression analysis fits of oil emission rate to water depth for the southern vents, northern vents, and combined T-10 Well Site. Data key on figure.

A least-squares, linear-regression analysis first order polynomial fit of E to D for both vents was calculated (Fig. 18) and was:

$E = -0.020\ D + 0.127;\ (E \geq 0)\ R^2 = 80.9\%$ Northern T-10 Vents (2)
$E = -0.087 D + 0.555;\ (E \geq 0)\ R^2 = 96.1\%$ Southern T-10 Vents (3)

where E has a minimum of 0 and R^2 is the correlation coefficient. The rationale for "clamping" E to zero is that if the water depth rises too high ($D > 6.38$, 6.35 m for the southern and northern vents, respectively), oil emissions would become negative, which is not physically possible – the ocean cannot be a source of oil to the subsurface. In reality, $E < 0$ represents the condition where the rising hydrostatic pressure forces seawater into the vent, causing a downwards oil and gas migration. However, given the definition of E - the oil flux that escapes into the ocean at the seabed into the water column – the oil flux cannot have a negative value. E for the T-10 Well Site was fit by:

$E = -0.099\ D + 0.645;\ (E \geq 0)\ R^2 = 97.2\%$ T-10 Well Site Total (4)

The improved correlation coefficient for the fit to the T-10 Well Site compared to the individual vents is consistent with connectivity between the two vent areas. Specifically, it indicates that some of the variability in the oil emissions for the individual vents was due to variations in the pathway of the seepage, not the total seepage. The fit for gas emissions, E_g, from the T-10 Well Site was:

$E_g = -1.284\ D + 8.707;\ (E \geq 0)\ R^2 = 92.5\%$ T-10 Well Site Total (5)

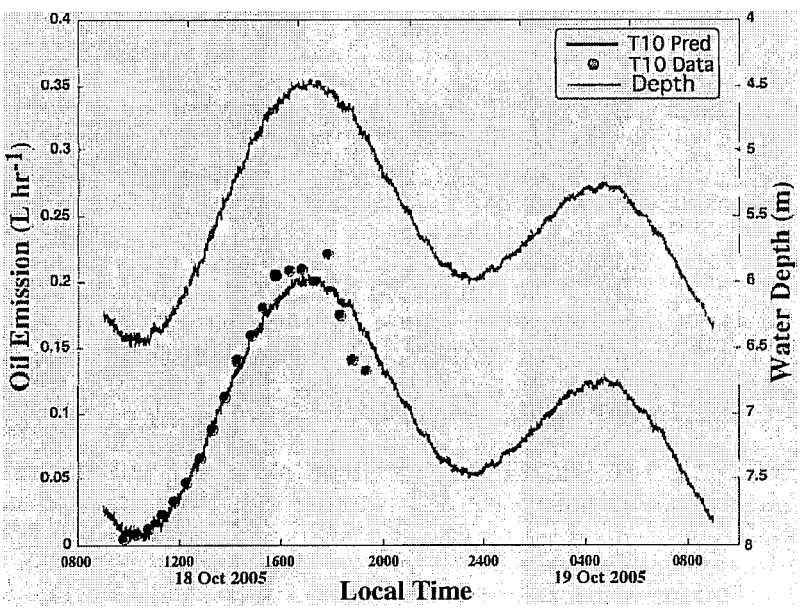

Figure 19. T-10 Well Site oil emission data and predicted from Equation (4), and water depth for 18-19 Oct. 2005. Data key on figure. See text for details on predicted oil emissions.

Using the fit for the combined T-10 Well Site emissions, equation (4), and the measured water depth from 0900 hours LT, 18 Oct. 2005 to 0900 hours LT, 19 Oct. 2005, the oil emission rate for the T-10 Well Site was calculated (Fig. 19). Naturally, the

predicted emissions follow the tide. Comparison with data was particularly good during the rising tide. The fit also highlights an asymmetry in the tidal response of oil emissions, with a faster decrease during falling tides relative to the predicted emissions. In fact, emissions for the T-10 Well Site peaked ~30 minutes after low tide. Integration of Eqn. (4) over the 24 hr. period beginning 0800 hours 18 Oct. 2005 yielded **total daily oil emissions for the T-10 Well Site of 2.37 L day^{-1}. Daily gas emissions over the same time period were 38.7 L day^{-1}** at STP for a daily average gas to oil ratio of 16 to 1. Note, at the seabed, the gas to oil ratio is lower due to hydrostatic pressure.

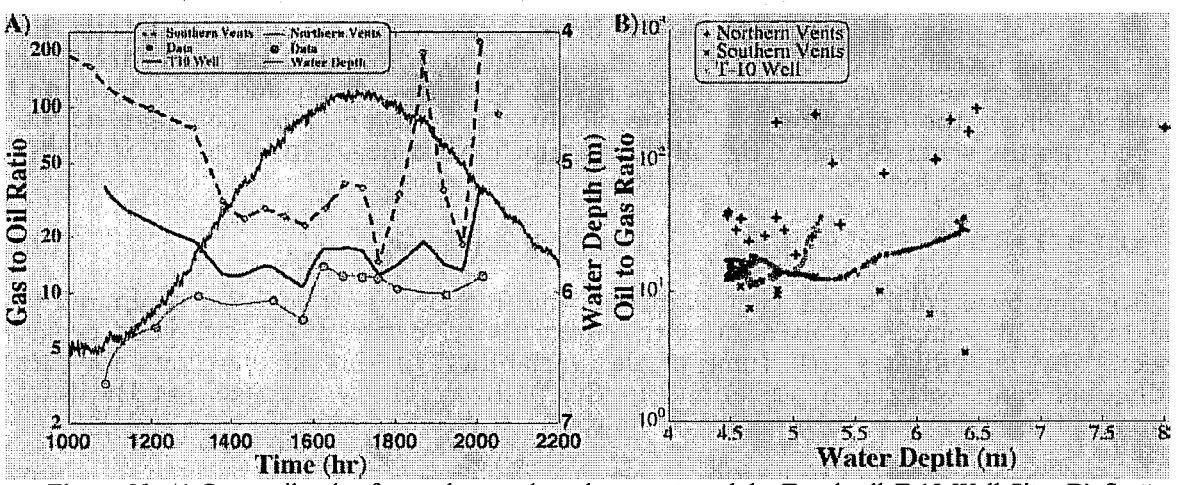

Figure 20. A) Gas to oil ratios for northern and southern vents and the Treadwell T-10 Well Site. **B)** Scatter plot of tide versus gas to oil ratios for data shown in A). Data key on figure.

4.3.3 Gas to oil ratios

Evidence for connectivity between the northern and southern vents at the T-10 Well Site is provided by the gas to oil ratios for the two vent areas (Fig. 20). At the beginning of the study period (high tide), the gas to oil ratio for the southern vents was decreasing rapidly from ~2 to 1. This suggests that southern vent emissions somewhat earlier were even oilier – emissions at high tide were much oilier than the average for the study – suggesting an oil slug had escaped. A similar event was observed during the 20 July 2005 cruise, although in that case, the sample jar overflowed. At the same time, emissions from the northern vents were much gassier than the mean for the study, 200 to 1. Over the next few hours, the gas to oil ratios of the two vent areas changed in the opposite direction – i.e., emissions for the southern vents steadily became less oily with the largest change during the ebbing tide. In contrast, emissions for the northern vents became significantly oilier at low tide – i.e., there was a clear decrease in the gas to oil ratio towards low tide followed by a noisy increase afterwards as the water depth increased. However, the combined gas to oil ratio shows far less variability. This is interpreted as indicating connectivity and is discussed further below.

5. SEA SURFACE SURVEY OBSERVATIONS

5.1 Spatial distribution of seepage sites

Sea-surface surveys were conducted using global positioning systems (GPS) from small boats and identified two seepage trends, one of which trended slightly towards shore in a generally east-west direction, and a second seepage trend that was in a generally north-south direction (Fig. 21). Also shown are the approximate historical locations of oil exploitation wharves in the vicinity of the Treadwell Wharf, including their approximate lengths. The north-south trend clearly is related to the location of the Treadwell Wharf. Note, lengths are approximate because the map showed distances relative to the bluffs, which certainly had eroded over the last hundred years. Connecting wharves are also shown.

The east-west seepage trend passed through an area of gas seepage ~300 m to the east-southeast, which was named the Sea Otter seeps (119° 35.81'W, 34° 25.02'N), and continued to the T-10 Well Site. To the east of the T-10 Well Site, the seepage trend appeared to intersect the Becker Intertidal seep (34° 25.189'N, 119° 36.219'W). Seepage along the approximately north-south trend only spanned a distance of ~100 m. At the T-10 Well Site and the S-4 Site, evidence of wells were found, thus it is likely that this trend identifies the location of the Treadwell Wharf. A sheen from a further seepage site ~50 m to the South of the S-4 Site is visible in the aerial image (Fig. 10) and is along the same trend. This site was not surveyed from the sea surface, but its position certainly suggests it also was related to drilling from the Treadwell Wharf, which extended offshore a distance of 375 m.

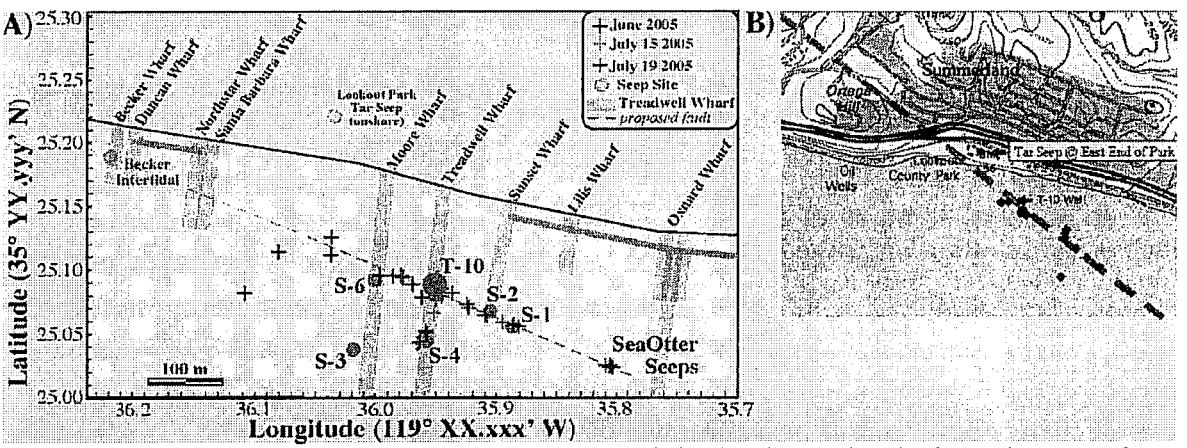

Figure 21. Sea-surface survey locations of oil and gas surfacing locations and study sites. Also, approximate location of Treadwell Wharf and other nearby wharves, all coordinates in NAD83, and the map is in uniform minutes – thus north-south distances in meters are slightly stretched. Also, note the locations of both ends of wharves are uncertain due to beach bluff erosion. Also shown is the location of the proposed Ortega Fault. **B)** Larger area view showing oil and gas surfacing sites, the T-10 Well Site, and the proposed Ortega Fault (dashed line), which passes to the north of Ortega Hill. (*Topo!*, 2001); Wildflower Productions). Wharf locations from *Golder Assoc.* (1995).

Site S-6 (34° 25.093'N, 119° 36.001'W, 16 ft water) was the site of a 1.3 m (4 ft.) diameter concrete cap, which in 2003 was observed to have an irregular asphaltic plug about 30 cm in diameter formed from a crack in the cap. Nearby was a 4 ft cubic block of concrete sitting on the seabed and protruding about a meter into the water column. Comparison with the historical location of the Moore Wharf indicates that it was on the Moore Wharf, and likely corresponds to a well passing through the proposed Ortega Fault. Approximately, 20 m to the North, at the approximate location of the intersection between the Ortega Fault and the Moore Wharf was an area with

significant surfacing oil. The seabed there was featureless sand, and probing with rebar by divers in March 6, 2007 did not find any concrete structures; however, the sand overburden was of unknown thickness.

5.2 Variability in oil sheens

Oil sheens in the Summerland area exhibited enormous variability on time scales from months (between different visits) to seconds. One source of variability is at the seabed, due to tides, temperature, swell, and other factors, which were addressed through seabed observations. However, sea-surface processes also are important sources of variability. Once the black bubbles reach the surface, they drift for a distance (at Summerland, typically, 5 to 20 m) before bursting and forming sheens. These include advection by currents, which are typically to the west and parallel to the shoreline. Breaking wind waves rapidly disperse the sheens. Winds also were observed driving the sheens towards shore or towards kelp beds. In the beach environment, during morning hours, winds typically are calm, becoming stronger later in the day in an onshore direction. Because currents typically are parallel to the shoreline, the combination of afternoon winds and currents have a high potential to advect sheens towards the shoreline.

5.2.1 Role of kelp canopies and oil sheens

Kelp canopies were also observed to affect variability in oil sheens. Overflights by the DOGGR and DFG-OSPR confirmed shoreline and on-water observations that kelp beds retained oil, providing temporary reservoirs and significantly affected the appearance of surface sheens. Fingerprinting of the COP seep field sheens showed that oil can remain trapped in the maze formed by kelp fronds floating at the sea surface and degrade significantly (Leifer et al., 2006). The kelp canopies also serve as "barriers" either temporarily protecting the shoreline from offshore oil sources and/or preventing nearshore or onshore oil sources (e.g., Becker onshore) from dispersing seaward. Oil trapped by the kelp canopy in the Summerland area can lose most of its volatiles.

Throughout the course of the Summerland studies, we observed during boat and beach surveys, that weathered oil sheens arising from the T-10 Well Site and other inshore and beach sources often accumulated within and along the inshore margin of dense kelp canopies when currents, tides, wind, and wave conditions were appropriate. Later in the day, when the tide rises, the kelp canopy sometimes became submerged. Then, typical wind patterns (onset of sea breeze) caused much of the oil trapped shoreward the kelp bed to be released and dispersed, the direction of oil movement depending upon prevailing winds and currents.

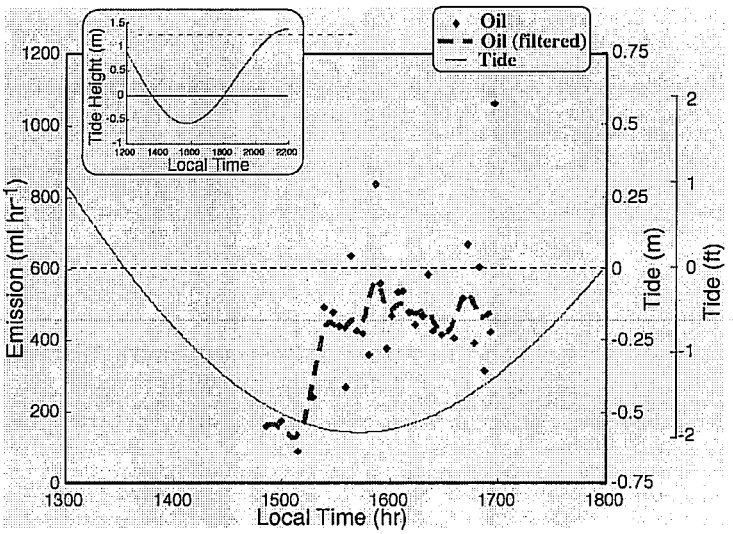

Figure 22. Oil emission rate (raw and 30-minute smoothed) for the Becker Onshore site with respect to time and tide height. Data key on figure. Inset shows tides over larger time range.

6. BEACH OBSERVATIONS

6.1. Oil and tar on Summerland Beach

The CSLC, USCG, and OSPR personnel conducted 50 onshore surveys of Summerland Beach to determine the extent of beach oiling from September 25, 2002 to 11 Mar. 2004. The beach at Summerland extends 2100 m (6900 ft) from Ortega Hill, on the west, to Loon Pt. on the east. The USCG surveyed the beach on 30 days, CSLC 19 days, and OSPR 4 days. Weathered tar balls, which ranged from 0.2 to 1-cm diameter, and fresh oil droplets were observed on Summerland beach (over a 1.8 km stretch) during 29 of 50 days (60 %). Tarballs and fresh oil droplets were always observed in less than trace quantities (<0.1% cover). Typically these tarballs were found in quantities ranging from one to several dozen and often were stranded by the tide among algal debris. Significant beach oiling incidents (defined as when more than 0.1% of the beach was covered by oil) were observed on only two of the 50 days surveyed.

6.2. Beach emissions

Oil emissions were measured on 8 Feb. 2005 at the Becker Onshore Site (34° 25.189'N, 119° 36.219' W - see Fig. 22) for 2 hours and 20 minutes during a period of negative tides using the petrolarium (see Fig. 9). We could only sample negative tidal periods were necessary as the site is only accessible at negative tide. The lowest tide was -1.7ft at 1547 hours Local Time. Oil emissions primarily originated from with an area of 2 x 3 cm. The oil emissions showed a rough inverse trend with tide height during the study period (Fig. 22). Mean emissions were 457±188 ml hr^{-1}, with the highest rate of 1.06 L hr^{-1}. Total daily emissions were extrapolated to a daily rate of 11.0 ± 0.46 Liters day^{-1}. Also, emission rates were still rising an hour after low tide.

7. SEABED SURVEY OBSERVATIONS

A seabed probing study July 2005 (Fig. 23) using brass rods searched for evidence of oil in sediments near the T-10 Well that might be correlated with larger scale geologic fault structures. Transects were conducted along compass directions of 0, 10, 30, 60, 180, 210, 280, and 350°, noted on the T-10 Well cement cap (see Fig. 23). The distance from the T-10 Well caisson of each probing is noted in centimeters to the left of each transect line. To the right is noted the depths at which oil was found below seabed grade. Also noted is the total depth of the unconsolidated sediment where less than 1 m below seabed grade. Where seabed probing released gas was noted by a "Y." In some areas, probing was only conducted to determine the absence of gas, noted by "N." Also noted on the figure is the location of the cone and tube tents and where a casing was found ~1 m east of the T-10 Well caisson, which was sticking out of the seabed.

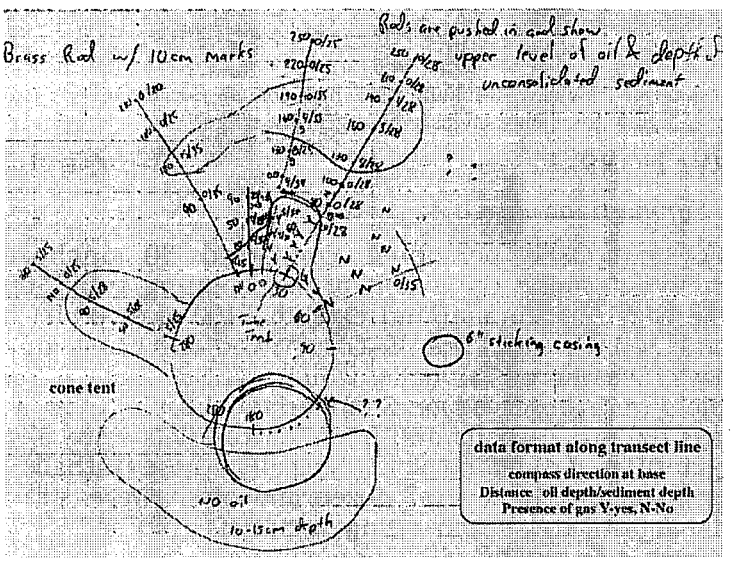

Figure 23. Results of seabed sediment probe survey, 20-21 July 2005. See text for description of data.

In general, the unconsolidated sediment was ~30 cm deep. Oiled sediment largely was much shallower generally 5 to 10 cm below seabed grade, and was often shallower. Overall, the seabed probing showed that seabed oiling only occurred within a short distance of each of the leaking seams on the T-10 Well caisson, extending almost two meters to the north-northeast from the T-10 Well caisson. No southward extension was noted. Oiled sediment also extended a meter and a half westward (280°), suggesting that the T-10 Well Site may develop a third area of seabed seepage. This also indicates that the caisson is most corroded along the northern seam. A repeat survey 18 Oct. 2005 did not find any evidence of oil emissions further from the T-10 Well caisson than the July 2005 survey despite the fact that the October seabed survey extended many meters to the north, as well as to the east and west along the direction of the seep trend (Fig. 21) and the proposed Ortega Fault.

8. GAS AND OIL GEOCHEMISTRY

Gas samples were collected from the southern vents during the 17 Oct. 2005 study at falling high tide - 12:05 Local Time (LT) - and low tide – 18:40 LT – and were analyzed. Two gas samples were analyzed by flame ion detection gas chromatography by Texas A&M GERG, one for low tide, and one for falling high tide - and one for rising tide shortly after low tide.

8.1 Gas analysis

The results in Table 3 show that the gas was almost entirely methane with trace higher n-alkanes, which increased slightly from propane (C_3H_x) to pentane (C_5H_{12}). More interesting is a shift towards higher molecular weight alkanes with decreasing tide, with ratios of the higher n-alkanes to methane increasing by factors of 2 to 3.

This was the same trend in gas to oil ratio for the combined T-10 Well Site emissions (oilier at low tide), but opposite to the trend in the gas to oil ratio for the southern vents (gassier at low tide). Of course, two data points in a highly variable system cannot be considered to demonstrate a causal relationship. However, the shift towards heavier n-alkanes with decreasing water depth was consistent across ratios of the lightest five n-alkanes measured. This is sufficiently supportive for the development of a testable hypothesis that will be the subject of future field studies.

Table 3. Analysis of gas samples from samples collected at the southern vents of the T-10 Well at high and low tide for 17 Oct. 2005.

Sample #	Time	tide ht (m)	CH_4 (%)[x]	C_2H_6 (%)	C_3H_x* (%)	C_4H_{10}** (%)	C_5H_{12} (%)
C3	12:05	6.1	99.3	0.49	0.15	0.024	0.042
C13	18:40	4.6	99.6	0.31	0.07	0.010	0.015
Mean			**99.4**	**0.40**	**0.10**	**0.017**	**0.029**
			C_2/C_1 -	C_3/C_1 -	C_4/C_1 -	C_5/C_1 -	
C3	12:05	6.1	202	683	5800	2340	
C13	18:40	4.6	321	1485	14300	6800	

[x] Percent is relative to total retrieved C_1-C_5.
*Propane (C_3H_8) and propylene (C_3H_6), **i-Butane and n-Butane

8.2 Oil analysis

A chromatogram was analyzed for sample C_3 and showed the oil was highly degraded (Fig. 24). This is unsurprising given the reservoir's shallowness and the likelihood of numerous pathways connecting the reservoir and the ocean along wells, fractures associated with natural seepage along the proposed Ortega Fault, and through shallow aquifers, that would allow microbes to enter the reservoir and biodegrade the oil. Sufficient oil was also collected to determine its density at 0.962 g cm^{-3}.

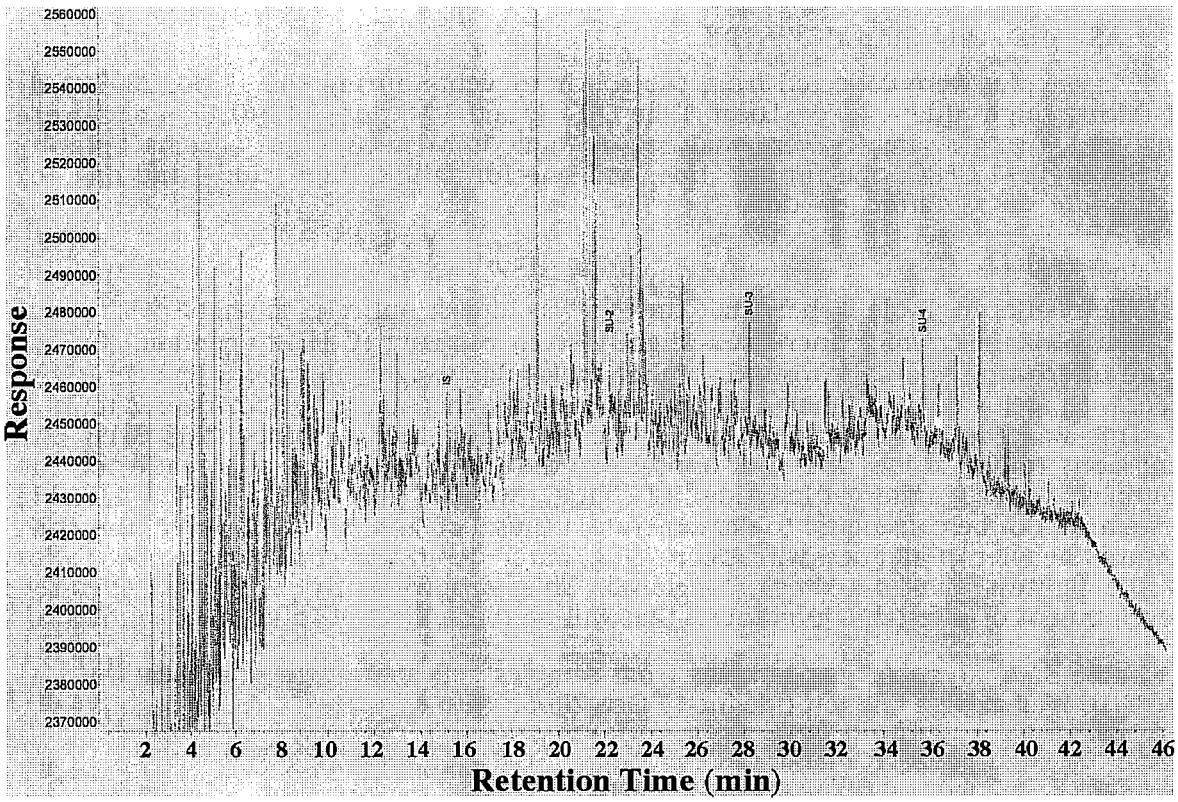

Figure 24. Chromatogram of an oil sample from Treadwell T-10 Well Site. IS is internal standard, and SU are surrogate compounds.

9. DISCUSSION

The Summerland oil study collected data for evaluating several hypotheses, the Treadwell-Ortega Fault Hypothesis, the Ortega Fault Extension to Seabed Hypothesis, the Tidal Seepage Response Hypothesis, the Vent Interconnectivity Hypothesis, the Oil Slug Flow Hypothesis, and the Observer Perception Hypothesis.

9.1 Treadwell-Ortega Fault Hypothesis

Study results strongly suggest that the Treadwell T-10 Well penetrated a fault. If true, this provides an explanation for the repeated failure of multiple abandonment efforts. To address this hypothesis, we used several approaches. Specifically, we collected historical data, geologic data, and mapping of the sea-surface spatial distribution of seepage offshore Summerland.

The hypothesis that Treadwell T-10 Well may have penetrated a geologic fault is based on evidence from studies in the Coal Oil Point seep field. There, studies show that seepage occurs along trends that are related to subsurface geologic structures including faults, outcroppings, and anticlines (*Hornafius et al.* 1999). In the COP seep field, sea surface surveys of the location of seepage generally are found along trends, which primarily are related to subsurface faults as well as other geologic features (*Marc Kammerling, Venoco Inc., Pers. comm., 2007*). Further, early prospectors (and the first offshore oil well in the world was drilled from the Treadwell Wharf at Summerland) tended to search for oil and drilling locations in regions of natural gas and oil seepage, which likely were offshore since oil deposits in the Summerland area are primarily located on the beach and offshore (Fig. 4). Onshore Summerland, shallow hydrocarbons are primarily gas deposits, which are consistent with reports of onshore gas seepage but not oil seepage. Thus, the historical data points to the feasibility of the Treadwell Fault Hypothesis.

Sea-surface surveys were conducted offshore Summerland using the approaches developed for the Coal Oil Point seep field and clearly identified a seepage trend of seepage aligned in an east-northeast trend (Fig. 21). This seep trend passed through the T10-Well Site and the S-4 Site. Given what is known about the orientation of Treadwell Wharf, slightly angled from perpendicular to the shoreline, the seepage trend perpendicular to the shoreline likely is from abandoned wells along the Treadwell Wharf.

Further support for the Treadwell Fault Hypothesis comes from a review of geological information for Summerland, including foremost the work of John Treadwell (Fig. 4), which shows oil accumulation primarily at the site of an unnamed fault ~400 ft offshore (~122 m), which corresponds approximately to the location of the T-10 Well Site, shown in Fig. 21. Note, that bluff erosion during the 20th century, suggests a slightly greater distance, plus there is uncertainty in where the base of the wharf was located historically relative to the bluffs. Further, geologic maps of the Carpinteria Basin (Figs. 2 and 3) shows the Ortega Fault with the same directional trend as the observed seepage trend, located slightly offshore Summerland and passing approximately through the location of the Treadwell T-10 Well Site.

9.2 T-10 Well Site, Ortega Fault Extension to Seabed Hypothesis

In addition to hypothesizing that wells on the Treadwell Wharf were drilled through a fault, indicated by John Treadwell's cross section maps as occurring at a depth of about 30 m, we propose that the fault extended to near the surface. In such case, seepage trends would be identifiable both near the T-10 Well as well as distant from it.

We conducted the seabed probing study to determine if there was a trend of oiled sediment with the same orientation as the sea-surface survey, east-west trend of oil and gas emission sites. However, oiled sediment was only found in the immediate vicinity of the Treadwell T-10 Well, located where the two seams of the metal caisson. With the most extensive oiling of sediment found off the northern vents on the outside of the caisson. Because after tent emplacement, sheens at the sea surface essentially stopped, we contend that this oiled sediment area was not actively emitting. The absence of a larger trend extending from the T-10 Well cap suggests that oil emissions in the study site are related to the T-10 Well Site, rather than the larger scale seepage trend. The presence of oiled sediment to the west suggests an alternate pathway is forming for oil to escape the Treadwell T-10 Well, outside of the northern side of the caisson (the northern vents are inside). If such a pathway forms, it likely would have a lower resistance, perhaps comparable to that of the southern vents. In such case, oil emissions from the two vents would become more equal. This could lead to slightly higher emissions; given that the total near-seabed surface resistance is high.

Thus, the seabed probe study did not confirm the presence of a seepage trend in the vicinity of the Treadwell T-10 Well at the seabed grade. However, this does not disprove the hypothesis. For example, given that the fault is tilted and the offshore side of the fault is up-thrusting, while the onshore component is down-thrusting (Fig. 3), the interaction between the vertical Treadwell Well and the tilted fault would significantly stress the seepage pathway along the well. However, these fault motions need not necessarily create seepage pathways in the immediately adjacent rock layers and deposited alluvial material.

Another area of notable oil emissions was located 30 meters south of S-6, at the approximate location of the Ortega Fault, and the historical location of the Moore Wharf. Although no research was conducted into the location of wells, comparable to Treadwell Wharf and the T-10 Well, it is likely that conditions are similar. As a result, due to the interconnection likely provided by the Ortega Fault, this area must be considered as a likely area for an increase in seepage should the Treadwell T-10 Well become sealed.

9.3 Tidal Seepage Response Hypothesis

The **tidal oil response hypothesis** states that decreasing hydrostatic pressure resulting in a relative increase in sub-seabed the overpressure, which drives seepage as it rises from the reservoir along pathways to the seabed. To test the tidal oil response hypothesis, two tents were deployed at the T-10 Well Site over a tidal cycle. The tents were positioned to capture all the oil and gas emissions from the site, in sample collection jars, which were periodically retrieved and replaced. Analysis of the data showed a strong response in the emissions to tidally driven changes in hydrostatic pressure. The proposed mechanism is that, while the hydrostatic pressure drops due to a decrease in tides, the pressure in the fractures, at first, remains constant. This leads to a greater overpressure and increased emissions. Increased emissions relieve the built-up overpressure in the seabed, eventually causing the emissions to decrease. For a rising tide, the opposite process occurs.

To gain better insight into the relationship between tides and seepage, we introduce an electrical network conceptual model of seepage (Fig. 25). In this model, electrical circuit components are analogs for physical components in a system of seepage. This model can also be used to infer physical aspects of the seep system, and was introduced in *Leifer and Boles* (2005a) based on observations from a three-tent network of gas seep tents deployed in the Coal Oil Point seep field.

In the simplest version of this model (Fig. 25A), the flow of oil and gas are driven by a reservoir pressure (V_r), greater than the seabed hydrostatic (emission) pressure

(V_e), creating an overpressure or driving voltage (V_r - V_e), across fractures with resistance, R. The resistance is equivalent to the viscosity. Thus, for a given driving voltage, there is a flow, which is equivalent to an electrical current, i. This flow passes through fractures, which have both resistance and a physical volume or capacitance, C. Then, the flow through for a seepage system, such as the T-10 Well Site, can be represented by a simple capacitor and resistor network. The electrical concept of ground represents the reference, oil-free environment, and is referenced to local hydrostatic pressure. A voltage only drives a current (flow) if it is above hydrostatic pressure.

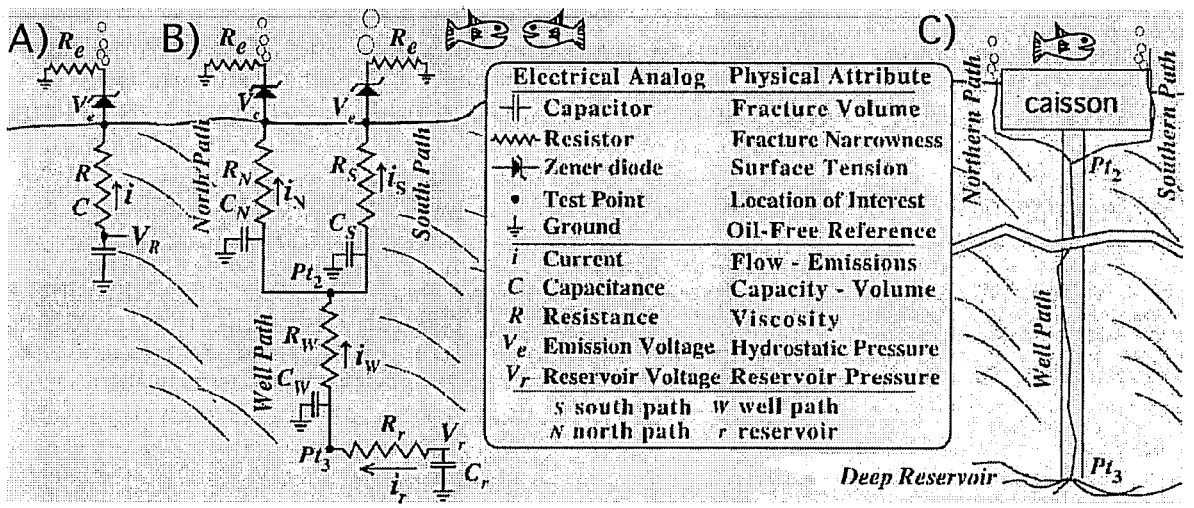

Figure 25. A) Simple schematic of electrical circuit conceptual model of seepage. Components and symbols defined on figure, and physical analogs. **B)** Electrical circuit conceptual model for the T-10 Well Site. **C)** Analogous schematic of the Treadwell T-10 Well Site seepage pathways.

An additional complication is that bubble formation at the seabed – i.e., seepage – requires an overpressure above hydrostatic to overcome pressure from the surface tension force. This is represented in the seepage model by a Zener diode, which has a fixed voltage (pressure) drop across it.

For the T-10 Well Site, data suggest greater complexity than the single resistor and capacitor network. Specifically, the two connected seepage vent areas suggest the simplified network shown in Fig. 25B, which corresponds to the physical system shown in Fig. 25C. In this model, there is a low resistance well pathway from the reservoir to near the surface, which is associated with the (likely highly corroded) well pipe casing. In the reservoir, it is hypothesized that there are numerous, higher resistance (R_r) migration pathways to the well pipe opening(s) through the oil-sand layer, simplified as a single opening (Pt. 3). The reservoir has much higher capacity (C_r) than the seepage system - i.e., $C_r > (C_W + C_S + C_N)$. The reservoir to seabed migration pathway bifurcates at some point (Pt. 2). From there, oil and gas complete their journey to the seabed through two high resistance, low capacitance pathways, either to the northern vents or the southern vents. Furthermore, it is highly likely that the bifurcation occurs close to the bottom of the concrete cap placed over the well. Note that, the bifurcation point (Pt. 2) represents a "bottleneck," above which flow resistance increases significantly, thereby at least partially isolating the upper seepage system (northern and southern paths from the lower seepage system (well path).

In this model, an increase in the hydrostatic pressure (V_e) leads to a decrease in the flow (i), while a decrease in V_e leads to an increase. Moreover, higher flow (i) discharges C (i.e., the fracture is drained) and as a result, the driving overpressure (V) across the fracture drops. However, this drop in voltage (pressure) leads to an increased in the flow (i) across the shallow fracture (R_S) – i.e., the shallow reservoir (C_S and C_N) are recharged from the "deeper" well reservoir (C_W and C_R). Leads to an increase in the flow (i_W) through the well pipe (i.e., across R_W) into the shallow "reservoirs" – the northern and southern paths. Other factors also could lead to changes in the flow, such as aquifer pressure increasing due to rain, or decreasing as aquifer levels drop (V_r) as well as changes in the reservoir system such as opening new pathways between different portions of the reservoir.

Based on this model, the higher flow from the southern vents can be interpreted as due to a lower resistance than for the northern vents. This is consistent with the fact that the southern vents are outside the caisson, and thus, for at least part of their path above Pt. 2, are constrained on one side only by sand/unconsolidated sediments and potentially tar deposits in the near seabed layers. In contrast, the northern vents are inside the caisson, and thus are constrained by a metal wall and concrete.

The capacity of the northern and southern paths can be compared by looking at the time delay between low tide (the forcing signal on V_e) and the peak in emissions (i). Specifically, the northern and southern pathways have response time constants, R_NC_N and R_SC_S, respectively. If the RC time constant is relatively long, then a rapid change in hydrostatic pressure (V_e) has negligible effect on the flow (i) because the vent cannot respond. In contrast, if RC is short, then the system responds rapidly, but could easily discharge (i.e., depressurize), leading to an asymmetry in emission response.

For both northern and southern vents, data show an asymmetry in the emission response to the tides, with a more rapid decrease for rising tide than the increase for the falling tide. This is consistent with depressurization of the pathways. Further, the time delay between peak oil emissions and low tide is ~30 minutes for the southern vents although with a large uncertainty, perhaps a factor of two (Fig. 4), while for the northern vents, any delay is less than can be distinguished given the variability in the emission data. At low tide, 30 minutes represents a flux of ~120 ml (peak emission was 243 ml hr^{-1}), which we propose is a rough estimate of C_S for the southern vents. The northern vents show a clear asymmetry but no clear time delay. Given the proposition that the resistance of the northern path is much greater than the resistance of the southern path ($R_N \gg R_S$) and has a shorter time constant ($R_NC_N \ll R_SC_S$), the capacity of the northern pathway (C_N) must be significantly smaller than the capacity of the southern path (C_S). This is consistent with the lower flow (emissions were a quarter of the southern vents) for the northern vents, and the physical location of the vents, too. The southern path likely has much greater volume than the northern path because it would include interstitial space in the sand as well as fractures.

The data show that as the water depth decreased, the emission rate increased significantly for both oil and gas, although much more strongly for oil (Fig. 16). Because the entire emission site was tented, the observed changes could not be due to a decrease elsewhere. In particular, for a hydrostatic pressure change of ~50% (2 m in water with a mean depth of ~5 m), oil emissions changed by ~2000%. For a flow between two infinite reservoirs, this suggests that the bifurcation point is located at a hydrostatic pressure of about a fortieth the fraction of the change, i.e., ~5 cm. However, based on the physical description of the concrete cap, it is highly unlikely that the bifurcation occurs so close to the seabed. Further, if there were very shallow bottlenecks on both the north and south pathways (i.e., $R_B \gg R_A$), then the emissions through the north and south pathways would be uncorrelated – the two vents would be isolated by the high resistance bottlenecks. That the two pathways are

interconnected is demonstrated by the greatly decreased variability in gas to oil ratios for the T-10 Well Site compared to either the northern or southern vents (Fig. 17). This strongly argues against very shallow bottlenecks in the north and south pathways - the bottleneck must be at the bifurcation point (or deeper). This clearly suggests that C_W for the "deeper" reservoir (part or all of the well caisson) is finite - i.e., comparable to the flow during the decreasing tidal cycle - and that emissions at high tide represent flow from the depressurized northern and southern pathways - i.e., the shallow reservoir (C_N and C_S).

Based on the data, it is likely that the well resistance (R_W) is much lower than either of the shallow paths (R_S and R_N). If R_W was higher than R_N and R_S, then the change in hydrostatic pressure would be expected to cause a much smaller change in emissions, since the pressure at Pt. 3 is much higher, ~5 atm based on the reservoir depth, i.e., ~25 times the tidal driven hydrostatic pressure changes. This is highly plausible given the abandonment procedures that were used at the Treadwell T-10 Well, as well as the likelihood that in the intervening century, portions of the well casing and its "telephone/rag plug" corroded/decomposed significantly. As a result, the data are consistent with the well casing being a low resistance pathway from the reservoir to near the seabed.

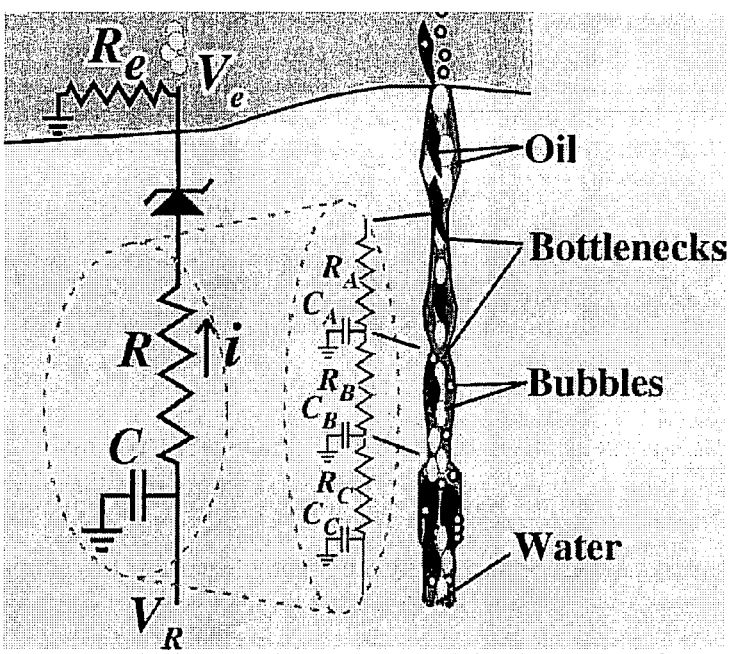

Figure 26. Conceptual electrical circuit model schematic of seepage illustrating how oil, with its higher viscosity (lower mobility) could find its shallower reservoir (CA) depleted due to bottlenecks which have less of an effect on gas, and which therefore has an effectively higher capacitance. Note, due to the viscosity of the oil, and the narrowness of the fracture, the gas and oil flow is described as slug flow rather than free, oily gas bubbles.

Of course, the representation of a pathway by a single resistor is a simplification. In reality, the resistance for a pathway is due to a series of flow bottlenecks. Physically, this can be interpreted as though R for oil in Fig. 25 is represented by a series network of resistors and capacitors (Fig. 26), which corresponds to a series of "bottlenecks between chambers." Each bottleneck slows the recharge of shallower chambers in the system from deeper chambers. Where a shallower chamber

bottleneck (R_A) is lower resistance than a deeper chamber (R_B), an increase in emissions from the shallower chamber is not replenished from deeper in the system as fast as the oil escapes. In this case, chamber A (C_A) rapidly becomes discharged, and is only slowly recharged through the deeper chambers, which have resistances R_B and R_C, from deeper in the fracture. Of course, a total resistance and capacitance can be calculated for the series of resistors and capacitors; which is why Fig. 25 is correct but simplified; however, by considering a network with greater complexity, as in Fig. 26, one notes that higher frequency changes in V_e should elicit a response in the system from shallower portions of the fracture, while lower frequency changes should provide information from deeper in the seepage system. Hence, if data were collected over a range of time scales, then frequency and phase analysis could serve to provide information from different regions of the seepage system.

Interestingly, the time delay between low tide and peak emissions for gas is significantly longer than for the oil (Fig. 16), particularly notable in the combined emissions (Fig. 17). From the conceptual model, this suggests that the *RC* time constant for the gas is longer than for the oil. Because of the lower viscosity of gas than oil and its ability to travel as bubbles (or more accurately slugs), bottlenecks (where the resistance originates) have less effect and *R* is lower. This would imply a greater capacitance for gas than oil, which is in agreement with the gas to oil ratio. However, the two phases clearly affect each other. The presence of oil decreases the volume available for free gas, while increasing the resistance to gas migration. Thus, an increase in oil flow decreases *C* for the gas, decreasing the gas *RC* time constant. Of course, where the oil blocks a chamber, it greatly increases the resistance for the gas by forcing the gas to pass through the oil. This could be represented in the model as a transistor, where the current of oil, affects the current of gas.

Another interaction between the phases results from the dissolution of gas in oil. As a result, increased oil flux causes an increased gas flux (through degassing in the collection jar). However, our analysis approach did not measure the pressure in the jar and thus degassed-gas was not measured.

It should be noted that the physical characteristics of the seep system can change over time. For example, as asphalt is deposited in pathways, the resistance increases and the capacitance decreases. This increase in resistance leads to a greater voltage drop (pressure drop) across the portion of the pathway that has been blocked. These processes will lead to decreased seepage. If the pathway becomes entirely blocked there will be a significant increase in pressure behind the blockage, and seepage will then be forced to use other pathways. However, the pressure drop across the blockage could also "blow free" the asphalt, lowering resistance and increasing seepage. Increases in pressure can originate from within the seepage system, or from external forces, such as increased aquifer pressure. And finally, seismic processes can change the physical character of the seepage system, as would corrosion and decomposition of plugging materials.

9.4 Vent Interconnectivity Hypothesis

The vent interconnectivity hypothesis proposes that areas of seepage near the Treadwell T-10 Well Site are interconnected. As a result, in the event where one vent or seepage site becomes sealed due to formation of asphalt plugs, the seepage will find another escape pathway.

In fact, it was interaction between the phases that allowed the conclusion that the two northern and southern vents were connected. Specifically, the gas to oil ratios for the two vent areas responded to the tide by shifting in opposite directions. This could be explained if the increased resistance to gas flow in one vent from greater oil flow, caused the gas to preferentially use the other vent. Thus, as the northern vents became progressively oilier, the gas flow through the southern vents increased,

becoming progressively gassier. Moreover, the changes in oil and gas flow between the two were comparable, even though emissions for the southern vents were significantly greater than for the northern vents. This was demonstrated by the gas to oil ratio for the combined T-10 Well Site, which largely varied within a narrow range for most of the study period, even though gas to oil ratios for the north and south vents changed greatly (Fig. 20).

Interconnectivity on a larger scale could not be demonstrated definitively. Specifically, at different periods, either the S-3 Site, or the T-10 Well Site were active and the dominant emission source offshore Summerland. This is consistent with interconnectivity between the two sites, but could also be coincidental. Demonstration of interconnectivity would require simultaneous emission measurements at both two sites; however, as noted, they were not active simultaneously during the tent deployment studies. Further, it was only because two tents were used, rather than one large tent, that interconnectivity and oil slug flow was demonstrated.

9.5 Oil Slug Flow Hypothesis

In the extreme case of slug flow, the pathway completely fills with oil, temporarily blocking gas from flowing through the pathway. Thus, one effect of oil flow on gas flow is a cycle where the oil stops the gas flow - i.e., a slug of oil entirely blocks the pathway - until pressure behind it increases above the resistance of the oil slug 'plug' and forces the oil out of the seabed. Then, the oil is followed by depressurization of the temporarily trapped gas behind the oil slug. The occurrence of slug flow is important because emissions (oil and gas) during slug flow are very different from mean emission rates. Thus, care is required to confirm that daily rates extrapolated from measurements did not occur during slug flow.

In fact, the effect of oil flow on gas flow can lead to a run-away effect where the oil stops the gas flow - i.e., a slug of oil entirely blocks the pathway until pressure behind it increases above the resistance of the oil 'plug' and forces the oil out of the seabed, allowing the trapped gas to flow freely from the seabed until the volume of gas trapped behind the plug is expelled into the water column. Just such an event was observed 20 July 2005 (Fig. 15), when one of the jars on the tent covering the southern vents overflowed. Although the overflowing of the 500-ml jar prevented any gas measurement, gas to oil ratios before were 1 to 1, far oilier than any measurements recorded. A decrease in the gas to oil ratio for the northern vents was also observed, suggesting that the slug of oil originated deeper than the bifurcation (Fig. 25, Pt. 2); with most of the oil escaping through the southern pathway. Evidence that the increase and decrease in oil emissions from the northern vents was not driven by tides is given by the gas emissions which showed negligible variability with tide - which changed little over the study period. In fact, the two gas emission rates measured for the southern vents on 20 July 2005 also were highly similar.

Based on the observations for 20 July 2005, the low gas to oil ratio at high tide on 18 Oct. 2005 (Fig. 20) is consistent with the tail end of a slug flow. Meanwhile, the gas to oil ratio for the northern pathway was significantly above the mean gas to oil ratio. Evidence that the changes in gas to oil ratios for each vent area largely was not driven by tides is provided by gas to oil ratio for the T-10 Well Site, which showed far less variability than gas to oil ratios for either vents individually. Thus, the system acted like a fluid (oil and water)-gas separator at low flow rates (high tide) but not at high flow rate (low tide). A possible explanation is that the bottom of the cement cap is rough with openings where oil and gas accumulate in a shallow "cap reservoir," before exiting into the two pathways, north and south. If we further speculate that the entry to the southern pathway from the "cap reservoir" is lower than the northern pathway entry, then if the oil and gas separate, they will escape through

different exits and hence pathways. In such case, the gas to oil ratio would depend on the ability of the oil and gas phases to separate, which requires some amount of time. At higher flow rates there would be less separation. This hypothesized model could be tested through the collection of data over a longer time period, and correlating gas to oil ratios with flow rates for the two vents over several tidal cycles.

Further, had only one portion of the T-10 Well been covered, then, the measured trend in oil to gas ratio with respect to tides would have been in the wrong direction. For example, the T-10 Well Site exhibited a shift towards oilier (lower gas to oil ratio) emissions with decreasing tides. However, emissions from the southern vents became less oily with decreasing tide. Thus, if only the southern vents were covered by a tent, the relationship between tides and gas to oil ratio would have been the opposite of the T-10 Well Site. Similarly, if measurements occurred only for a short time during a period of slug flow, as occurred 20 July 2005, flow rates that are highly unrepresentative of mean flow rates would be measured.

9.6 Observer Perception Hypothesis

We propose that perception plays a significant role in oil emission estimates where direct quantification as in this study is not undertaken. There are many reasons that can lead observers to over-estimate oil emissions.

Observer perception results in varying estimates and/or concentrations of oil seepage, sheens, and beached oil. It is because of perceptual differences, that anecdotal estimates often do not correctly reflect oil emissions. Factors affecting oil estimates include, but are not limited to: oil emissions, including the timing of transient emissions, glare conditions, viewing angle and direction, presence/absence of kelp canopies, swell and wave height and period, currents, and winds, level of human activities, and the methods used to quantify emissions, as well as the experience of the observers.

Using observations, like the gross appearance of 'oil droplets', which do not take into consideration gas to oil ratios, can lead to overestimates of oil quantities. Similarly, estimations of the amounts of beached oil in the form of black foamy mousse by untrained observers can lead to gross overestimates of oil discharge. The advection of sheens by winds and currents also can lead to either under- or over-estimation (unless the observer is experienced in interpreting the observations).

The perception of oil sheens and beach oiling, of course, also can depend upon the level of human activities occurring at the same location (beach) and time as oil sheens and mousse appear. Although Summerland beach is a popular recreational location, OSPR is aware of only three Hazardous Materials Spill Reports to the Governor's Office of Emergency Services (OES Spill Reports) originating from this beach during the last 12 years - in 1992, July 2003, and Feb 2005. In these reported oiling incidents, the beach had oily mousse stranded in the swashline at high tide. In all cases, oil released from the Becker Intertidal Seep appeared to be the primary source of the mousse.

The most important factors to the perception of oil (aside from its presence) are the timing and location of human activities, i.e., whether they are concurrent with conditions that transport oil towards inhabited areas during daylight hours. There are three distinct viewing scenarios, beach and bluff, on-water (kayakers and boaters, surfers, fisherman, etc.), and aerial. Furthermore, since oil and gas emissions are not constant and conditions vary, infrequent visitors to the area during periods of larger emissions (visible sheens) likely will assume such emissions are representative. Observing conditions, such as viewing angle, lighting angle and intensity can also affect the perception of oil on the sea surface. Thin sheens are only visible at certain viewing and illumination angles.

9.6.1 On-water and in-water activities

During the recent studies and historic observations, divers observed small 'B-B' sized 'oil' droplets, termed black bubbles in this study, rising to the sea surface from the seabed. Divers also noted them drifting along the seabed in recent surveys. Oil droplets on the seabed must have contained sediment given the oil density of 0.963 g cm^{-3}, and also likely contained small bubbles. Where black bubbles were rising, although they appeared to be pure oil, their rise rate was too fast for pure oil (particularly given that the oil's specific gravity was 0.973), leading to the suspicion that they were gas bubbles heavily coated with oil. Black bubbles generally drifted with the current just under the water surface for a distance of tens of meters before bursting and releasing oil sheens. As demonstrated in this study, measured gas to oil ratios showed that overall emissions were primarily gas. *If the droplets were pure oil, our total seepage estimates would have been higher by one to two orders of magnitude.*

Also, kelp canopies in the Summerland area can detain oil on the shoreward side of the kelp bed at low tide when the surface canopy is at its densest. This oil may be released, either moving shoreward or seaward depending upon winds, currents, and sea conditions. This can lead to widely varying perceptions among observers of the total oil emitted.

9.6.2 Beach activities

For oil to be observed on the beach, it must be either advected towards the beach in sufficient quantities to pass through the surf zone or must be discharged within or inshore of the surf zone from intertidal sources. The general absence of OES Spill Reports of beach oiling suggests that these conditions are not frequently met. Oil sheens and sheens beyond the surf zone can be observed from the beach, but generally only under certain lighting conditions. As a result, sheens are difficult to observe from the beach or the cliffs due to the shallow viewing angle and glare.

10. IMPLICATIONS AND CONCLUSIONS

Studies off shore of Summerland identified likely locations of faults, trends of natural seepage, and man-made oil related facilities. Consideration of the data strongly suggests that the Treadwell T-10 Well, which was abandoned three times, was drilled into a fault zone. Although we have no way of knowing what oil and gas emissions from the T-10 Well Site were prior to abandonment efforts, small discharges occur at the site on an intermittent basis. Therefore we propose that any future abandonment efforts are unlikely to meet with greater long-term success as has been the case with recent and historical abandonment efforts. We propose that small-scale seepage eventually will become evident due to natural seismic related processes.

Deployment of two specially designed seep capture tents at the Treadwell T-10 Well Site, provided the first high quality quantitative time series of marine seep oil emissions. Data clearly showed a tidally driven variability in the oil and gas emission rates. Estimated total daily emissions were ~2.4 liters oil per day based on a relationship between tides and oil emissions. Gas to oil ratios were ~16 to 1, i.e., most of the black oily bubbles escaping at the seabed, which appeared to contain significant oil, were in reality primarily gas.

Data were further analyzed in terms of an electrical circuit network, which suggested that the connection between the two vents occurred quite shallowly, and that the well casing provided a relatively low resistance pathway compared to the pathways around the concrete cap near the seabed. The electrical circuit was used to non-invasively (no environmental impact statement needed) infer details of the subsurface seepage.

However, given the shallowness of the reservoir, it is unlikely that large oil emissions will arise from the capped T-10 Well Site in its current condition. Although, a significant increase in aquifer pressure could cause an increase in oil and gas emissions, due to the shallowness and isolated nature of the oil reservoir, any increases would be small and short-lived. Further, the oil emissions would be small, relative to other natural oil sources in the Santa Barbara Channel, specifically, the Coal Oil Point seep field. Dramatic increases in aquifer pressure, though, could result in the opening of partially or completely sealed pathways, or opening new pathways, and could temporarily alter the resistances and capacitances of the seep system.

One of the important study conclusions was that observer perception can significantly affect perceived emissions of oil, and lead to qualitative emission estimates highly divergent from quantitative emission measurements.

Observations were consistent with interconnectivity between the Treadwell T-10 Well Site and the S-3 Site, likely associated with the historical Moore Wharf, although the observations did not prove the hypothesis. Further, given the location of the Ortega Fault, the presence of surfacing oil from the Site S-6, it is likely that this area is interconnected with the Treadwell T-10 Well. Thus, we propose that this area be designated a "risk area" for increased seepage should the Treadwell T-10 Well cease seeping due to development of an asphaltic plug or other reasons.

Analysis of the gas to oil ratios demonstrated interconnectivity between vents on the north of the Treadwell T-10 Well Site, and the south of the Treadwell T-10 Well Site, validating the approach.

It should be noted that throughout the multiyear study period, no oiled wildlife was observed in the Summerland beach area.

Three peer-reviewed manuscripts were published based on this research:

Leifer, I and K. Wilson. 2007. Tides and the Emission of Oil and Gas from an Abandoned Oil Well: Nearshore, Summerland, California. *Marine Pollution Bulletin, In Press.*

Leifer, I., and K. Wilson, J. Tarpley, R. Lewis, R. Imai, K. Mayer, and C. Moore. 2005. Factors affecting marine hydrocarbon emissions in an area of natural seeps and abandoned oil wells - Summerland, California. *Proc. Internat. Oil Spill Conf., May 15-19, 2005, Miami, FL*, EIS Digital Publishing, 14718A.

Leifer, I and K. Wilson. 2004. Quantified oil emissions with a video-monitored, oil seep-tent. *Marine Technology Society Journal*, 38(3), 44-53.

11. References

Arnold, R., 1907. Geology and oil resources of the Summerland District, Santa Barbara County, CA. U.S.G.S. Bull. No. 321

Boles, J.R., Clark, J.F., Leifer, I., and Washburn L., 2001. Temporal variation in natural methane seep rate due to tides, Coal Oil Point area, California. *Journal Geophysical Research* 106C11, 27077-27086.

Clift, R., Grace, J.R., and Weber, M.E., 1978. Bubbles Drops and Particles. Academic Press, New York/New York, pp 380.

Curran, S., 1995. Memorandum to Greg Scott State Lands Commission -16 March, 1995. Subject: Summerland Oil Well Abandonments - Re-evaluation, Min. Res. Mgt. Div. Unpub.

Fairweather Pacific LLC., 2000. Summerland Well Research Phase I and Phase II-A. Project Reports. November 2000, Unpublished.

Freckman, J.T., 1981. Pete Brumis Contract: Oil seep location and containment, Summerland Beach Area, Santa Barbara County. Mem. to D.J. Everitts, Chief State Lands Comm., 8 April 1981.

Giallonardo, T., and Koller. A., 1978. Gaviota offshore gas field. Calif. Div. of Oil and Gas. Pub No. TR21. 8.

Golder Assoc., 1995. Map and Dive Report. Geophysical interpretation magnetometer, side-scan sonar, and sub-bottom profiler data - Maps 1 and 2 - Report to PENCO/Margeophys CA - Dated 2/17/95. Unpublished.

Grosbard, A., 2002. Treadwell Wharf in the Summerland, California Oil Field: The first sea wells in petroleum exploration. *Oil-Industry History* 3(1), 1-19.

Hodgson, S.F., 1987. Onshore oil and gas seeps in California. California Division of Oil and Gas, Sacramento, CA. 97 pp.

Hornafius, J.S., Quigley, D.C., and Luyendyk, B.P. 1999. The world's most spectacular marine hydrocarbons seeps (Coal Oil Point, Santa Barbara Channel, California): Quantification of emissions, *Journal Geophysical Research-Oceans*, 104C9, 20703-20711.

Johnson, B.D. and Cooke, R.C., 1979. Bubble populations and spectra in coastal waters: a photographic approach. *Journal Geophysical Research* 92C2, 3761-3766.

Lammers, D.A, 1975. Internal memorandum to D.J. Everitts Removal of hazardous conditions - Summerland and Ellwood. Dated July 21, 1975.

Leifer, I., Luyendyk, B.P., and Broderick, K., 2006. Tracking an oil slick from multiple natural sources, Coal Oil Point, California, *Marine Petroleum Geology* 23(5), 621-630.

Leifer, I., and Boles, J., 2005a. Measurement of hydrocarbon flow through fractured rock and unconsolidated sediment of a marine seep. *Marine Petroleum Geology* 22(4), 551-568.

Leifer, I., Boles J., 2005b. Turbine seep-tent measurements of marine hydrocarbon seep forcing on second time scales. *Journal Geophysical Research* 110, C01006, doi:10.1029/2003JC002207.

Leifer, I., and Patro, R., 2002. The bubble mechanism for transport of methane from the shallow sea bed to the surface : A review and sensitivity study. *Continental Shelf Research* 22, 2409-2428.

Leifer, I., and MacDonald, I., 2003. Dynamics of the gas flux from shallow gas hydrate deposits: Interaction between oily hydrate bubbles and the oceanic environment. *Earth Planetary Science Letters* 210(3/4), 411-424.

Leifer, I., De Leeuw, G., and Cohen, L.H., 2003a. Optical measurement of bubbles: System, design and application. *Journal of Atmospheric and Oceanic Technology* 20(9), 1317-1332.

Leifer, I., De Leeuw, G., Kunz, G., and L. Cohen, 2003b. Calibrating optical bubble size by the displaced mass method. *Chemical Engineering Science* 58(23/24), 5211-5216.

Leifer, I., Wilson K., Tarpley J., Lewis R., Imai R., Mayer K., and Moore C., 2004. Quantified oil emissions with a video-monitored, oil seep-tent, *Marine Technology Society Journal*, 38(3), 44-53.

Lindbergh, J.M., 1961. An analysis of possible means of removing approximately 90 old oil well casings from the beach and nearshore area off Summerland, CA, Feb 10, 1961 In accordance with the State Lands Commission - W.O. 3399, Unpublished Report.

Mikolaj, P.G., and Ampaya, J.P., 1973. Tidal effects on the activity of natural submarine oil seeps. *Marine Technical Society Journal* 7, 25 - 28.

National Geographic, 1920 pg 188.

National Institute of Health, 2003, NIH Image Software, NIH Image ver. 1.62b30 (developed at the U.S. National Institutes of Health and available on the internet at http://rsb.info.nih.gov/nih-image/).

NRC (National Research Council), 2003, Oil in the sea III: Inputs, fates and effects, National Academy Press, Washington, D.C., pp 265.

Patro, R., Leifer, I., and Bowyer, P., 2002. Better bubble process modeling: Improved bubble hydrodynamics parameterisation. In *Gas Transfer and Water Surfaces*, Eds. M. Donelan, W. Drennan, E.S. Salzman, and R. Wanninkhof, AGU Monograph 127, 315-320.

PENCO, 1995. Summerland oil well abandonment project-summary of priority sites to CSLC and USCG, Vol. 3 Section 1 Unpublished Dive Report.

Sam, A., Gomez, C.O., and Finch, J.A., 1996. Axial velocity profiles of single bubbles in water/froth. *International Journal of Mineral Processing* 47, 177-196.

Topo!, 2001. National Geographic Maps, Evergreen, Colorado, 80437-4357.

USCG, 1995. Summerland Beach oil well abandonment. Letter from Captain E.E Page to interested parties. Dated 24 Feb. 1995. Unpublished.

Wilkinson, E.R., 1972. California offshore oil and gas seeps. California Division of Oil and Gas, Report No. TR08 Sacramento. 11.

APPENDIX A1 - VIDEO BUBBLE ANALYSIS METHODOLOGY

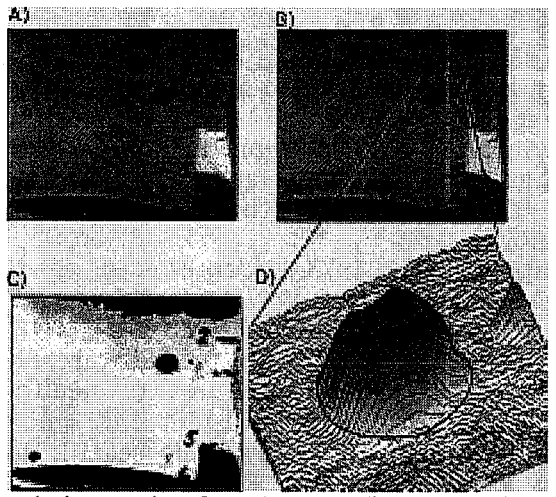

Figure A-1. Example of image analysis procedure for a 4770-μm diameter bubble with a thick oil coating rising in the collection jar. **A)** Original image. **B)** Extracted image. **C)** Thresholded image. **D)** Two-dimensional intensity profile of image subset indicated by dashed box on **B**.

Analysis of oil droplet video provided high time resolution flux series allowing calculation of the oil and gas mass transported by each bubble-droplet. Video was digitized into a series of frames (108,000 hr^{-1}). Navigation through the sequence of files, image processing, and basic analysis was by routines written in NIH Image (*National Institute of Health*, 2003). Fortunately, most frames were empty. Moreover, since the droplets rose slowly, droplet measurements were analyzed for each five frames in the sequence. This allowed a statistically significant number of measurements of each droplet to account for shape oscillations and noise. Frames with bubbles (Fig A-1A) were "extracted" (Fig. A-1B), a process in which each odd row of pixels was replaced with by interpolation of neighboring even pixel rows (*Leifer et al.*, 2003a). Extraction removed interlacing effects. The image was then thresholded – i.e., made binary (Fig A-1C) - at an intensity slightly above the background. Correctly choosing the intensity threshold was important, because the apparent diameter of the bubble decreased with increasing thresholding intensity. This can be seen in the cone shape of the intensity surface plot (Fig. A-1C). The threshold value used in Fig. A-1C is indicated in Fig. A-1D by a line. *Leifer et al.* (2003b) showed that the appropriate intensity is slightly below the background, because bubbles are surrounded by a bright halo created by off-axis reflected rays.

From this analysis, a time series of major and minor axes and x and y locations were produced. Since the units were in pixels per frame rate (30 frames sec^{-1}), a size scale was used to convert to centimeters. The variable length lens was set at 'wide angle', because poor water visibility prevented obtaining clear images unless the camera was very close to the collection jar. Thus the size scale varied significantly from 32 pixels cm-1 at the distant jar wall, to 48 pixels cm-1, at the jar's near wall,. This size uncertainty was minimized by noting whether droplets were in the near, center or

distant portion of the field of view and using the appropriate size scales. In this manner, size error was reduced to about ±7%. Further analysis was by routines written in Matlab (The Mathworks, Mass).

The bubble equivalent spherical radius, r, was calculated by

$$r = \sqrt[3]{r_1^2 r_2} \tag{A1}$$

where r_1 was the major radius, and r_2 was the minor radius (*Sam et al.*, 1996). Bubbles were tracked through the frame sequence, and measurements of r for each bubble were averaged together.

The size distribution, Φ, of all oily bubbles was determined by size segregating the time series of radii into logarithmically spaced bins, normalizing to per unit radius increment and per time interval (i.e., the number of seconds analyzed). Error bars were calculated from the square root of the number of bubbles in each radius bin. Bubble distributions were generally described by a power law dependency - e.g., *Johnson and Cooke (*1979)

$$\Phi(r) = k\, r^{-S} \tag{A2}$$

where S was the power law exponent and k was a constant. Values of S were calculated by a least-squares, linear-regression analysis of the log of both sides of (1) over an appropriate size range.

Leifer and Boles (2005a) observed with a video based bubble measurement system, a bubble stream from a single vent which produced a narrow, peaked Φ whose peak radius varied about 10% with an approximately 4 Hz period. They interpreted this variation as due to changes in vent mouth size due to varying oil coating, i.e., the oil and gas fluxes vary in time and not in parallel. Bubble sizes within the field of the camera were larger than at the seabed due to the decrease in hydrostatic pressure. Bottom depth was 5.2 m water where the tent was deployed, however, camera observations were recorded at a depth of 3.2 m. Thus using Boyle's law, $P_1 Vol_1 = P_2 Vol_2$, and the volume of a sphere, $r_2 = r_1 (P_1/P_2)^{0.33}$. For P_1 = 1.32 Atm and P_2 = 1.52 Atm, the maximum increase in bubble size from the seabed to collection jar was 4.8%. This was an upper limit because some fraction of the bubble volume was incompressible oil. Thus, as the bubble oil content increased, the gas fraction that underwent hydrostatic expansion decreased. A second factor that may have induced bubble growth was oil outgassing. Absent data on the dissolved gas pressure in the oil, we assumed that the gas and oil were equilibrium at the seabed. For the very low oil flow rates, this assumption may have been reasonable because of the residence time in the sediment overburden before escaping at the seabed.

Leifer and Boles (2005a) observed a variation in Φ and bubble V_B, which they interpreted as consistent with varying oil content on different bubbles. Rise velocity was calculated from the vertical distance between bubble locations in subsequent frames. Bubbles were tracked through the

frame sequence, and the measured V_B, for each bubble averaged together. *Leifer and Patro* (2002) calculated parameterizations for hydrodynamically "clean" and hydrodynamically "dirty" bubbles. Dirty bubbles were those contaminated with surfactants (surface-active substances, which were compounds or particles that had both hydrophobic and hydrophilic sites) and thus "preferred" air-water interfaces. A bubble in contaminated water behaved hydrodynamically clean if the amount of surfactant was insufficient for the bubble size. *Patro et al.* (2002) showed that in seawater, bubbles larger than 1500 μm behaved clean. Oil reduced the bubble rise velocity (by reducing the buoyancy), the decrease in rise velocity was related to the amount of oil. V_B ratios were calculated for each bubble in comparison with the dirty bubble V_B parameterization for the same radius. Comparison with predicted rise velocity for non-oily bubbles allowed estimation of the mass of oil necessary to decrease the rise speed and thence the oil to gas ratio. V_Bw as determined by tracking bubbles between frames and using the size scale to convert the velocity from pixels per frame to centimeters per second.

The bubble V_B is a balance between the drag and buoyancy forces, where the buoyancy force is driven by the density difference between the water and the oily bubble. There is no simple expression for the drag force, except for very small and slow rising bubbles where the flow around the bubble is laminar ($Re < 1$, where Re is the non-dimensional Reynolds number and is defined $Re = 2rV_B/\nu$ where ν is the kinematic viscosity of water) at higher Re, details of the turbulence wake and bubble shape are important. To estimate the oil mass on the bubble, we looked at the decrease in rise velocity due to decreased buoyancy. Buoyancy affects the rise velocity as the density difference between the water and the bubble (and oil), and is expressed for laminar flow bubbles ($Re < 1$) by Stokes rise velocity, $V_{B\text{-}ST}$, which is (*Clift et al.*, 1978)

$$V_{B-ST} = \frac{2}{9}\frac{gr^2}{\nu}(\rho_W - \rho_B) \qquad \text{(A3)}$$

where g is gravity, ρ_W is water density, ρ_B is the bubble density. For a pure gas bubble, $\rho_W \gg \rho_B$, and is ~1, although with increasing oiliness, ρ_B increases and ρ_W - ρ_B decreases. (1) can be solved for ρ_B and then using the bubble volume ($4/3\ \pi r^3$), the bubble mass, m_B, (both oil and gas) can be calculated assuming that the oil density is known. The problem with using Stokes V_B is that it is inappropriate for the bubbles observed which had large values of Re. Instead, we solved for m_B, using the ratio of observed and predicted - dirty, non-oily $V_B(r)$ - rise velocities. We assumed that oil-coated bubbles behaved hydrodynamically dirty (*Leifer and Boles*, 2005a). Based on equation A2, we related the ratio of density differences to the ratio of the rise velocities

$$\frac{V_B}{V_{B-Dirty}} = k\frac{(\rho_W - \rho_B)}{\rho_W} \tag{A4}$$

where k is a function of radius that describes that as oil increases on a bubble, the decreasing buoyancy causes V_B to decrease, which further decreases the drag; which reduces the amount V_B decreases. For Stoke's rise, $k = 1$, but for higher Re, $k < 1$. In (3) the bubble density for the non-oily dirty V_B was much less than ρ_W and was neglected. Equation (3) can be solved for ρ_B, which is simply the bubble-droplet mass, M_B, divided by its volume

$$\frac{\rho_W}{k}(1 - \frac{V_B}{V_{B-Dirty}}) = \frac{3M_B}{4\pi r^3} \tag{A5}$$

or

$$M_B = \frac{4\pi r^3 \rho_W}{3k}(1 - \frac{V_B}{V_{B-Dirty}}) \tag{A6}$$

Once the oil volume is determined with the oil density, ρ_{oil}, ~ 0.975 g cm^3 for reservoir oil in the Summerland area (Bill Castle, California Dept of Fish and Game, Office of Spill Prevention and Response -Pe rsonal Communication, 2004), the gas volume is calculated by subtracting from the total bubble volume,

$$Vol_{GAS} = Vol_{\mathbf{B}} - Vol_{OIL} = \frac{4\pi r^3}{3} - \frac{M_B}{\rho_{OIL}} \tag{A7}$$

APPENDIX A2 – DETAILED GEOLOGIC MAP OF SUMMERLAND AREA

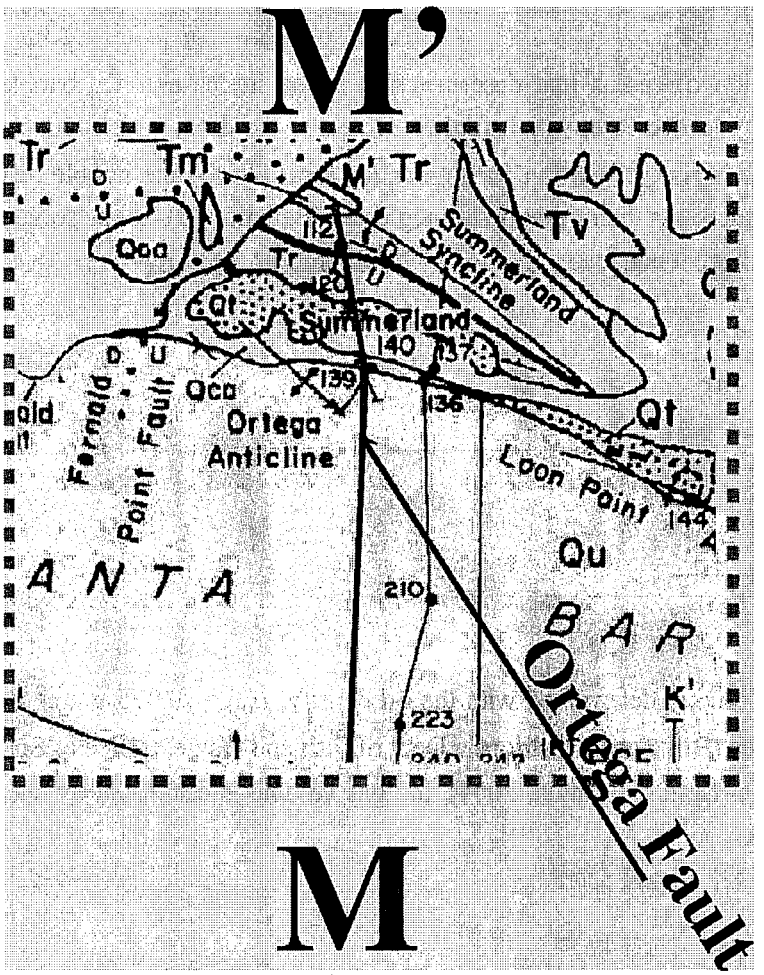

Fig. A2 – Enlarged geologic map of Summerland area.

APPENDIX A-3 PHOTOS FROM THE SUMMERLAND STUDY

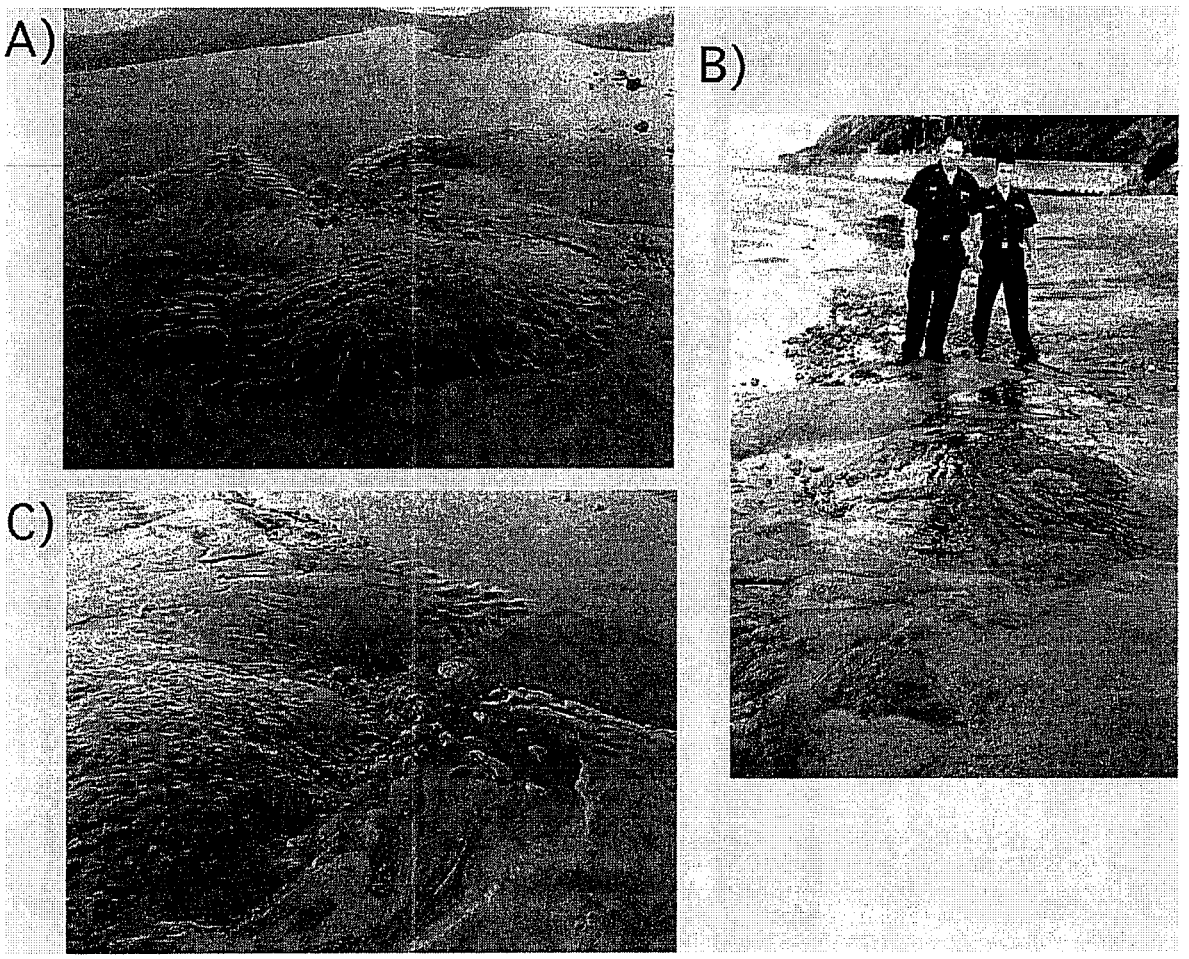

Fig. A3-1. Photos of Becker Onshore absent sand overburden from different viewpoints. Oil seeped from oil bearing rock formation and accumulated in a tide pool. Becker Onshore is located below the west end of Lookout Park at Summerland Beach. A) Among the oil sources is an 18 cm diameter vent immediately below and right of photo center. As tide rose, oil in the tidepool entered the surf, wave action formed oil mousse, which was carried downcoast by longshore current and stranded on approximately 0.7 miles of beach. A) and C) - courtesy of the U.S. Coast Guard, Marine Safety Detachment, Santa Barbara). B) US Coast Guard Safety Detachment personnel. (Photo B taken by Ken Wilson on July 15, 2003)

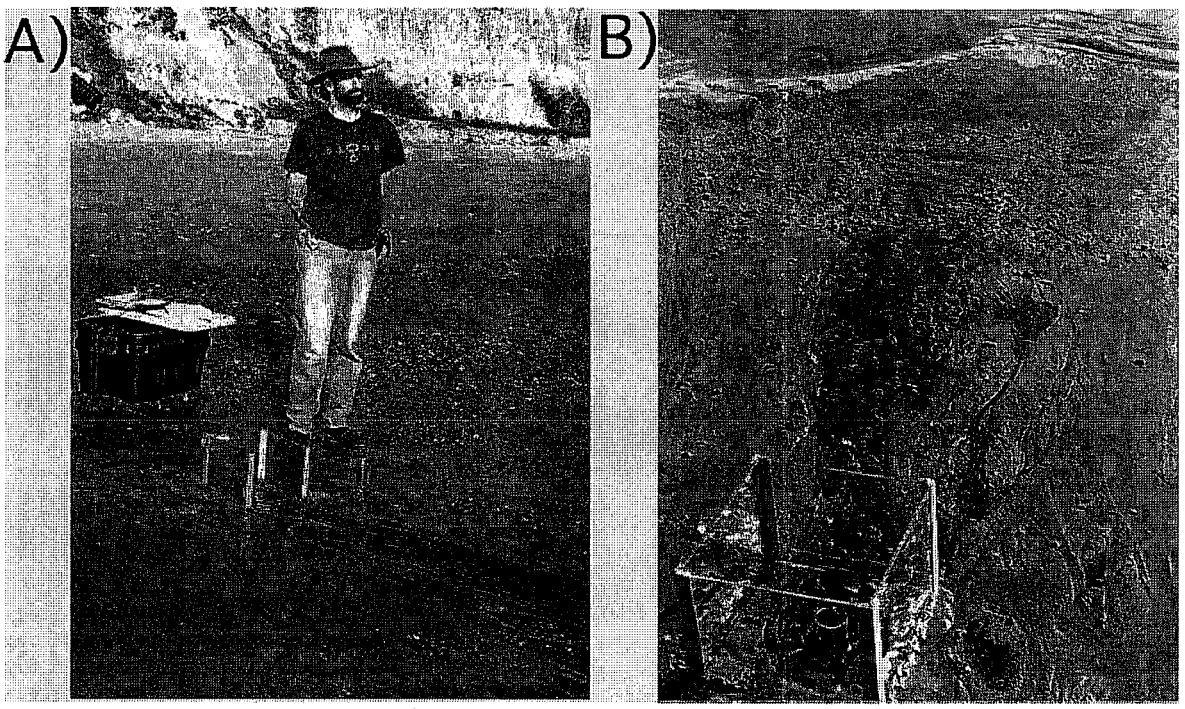

Fig. A3-2. Photos of petrolarium at Becker Onshore with sand cover. A) Scientist Ira Leifer. B) Oil escaping from seep when petrolarium first placed on the seep.

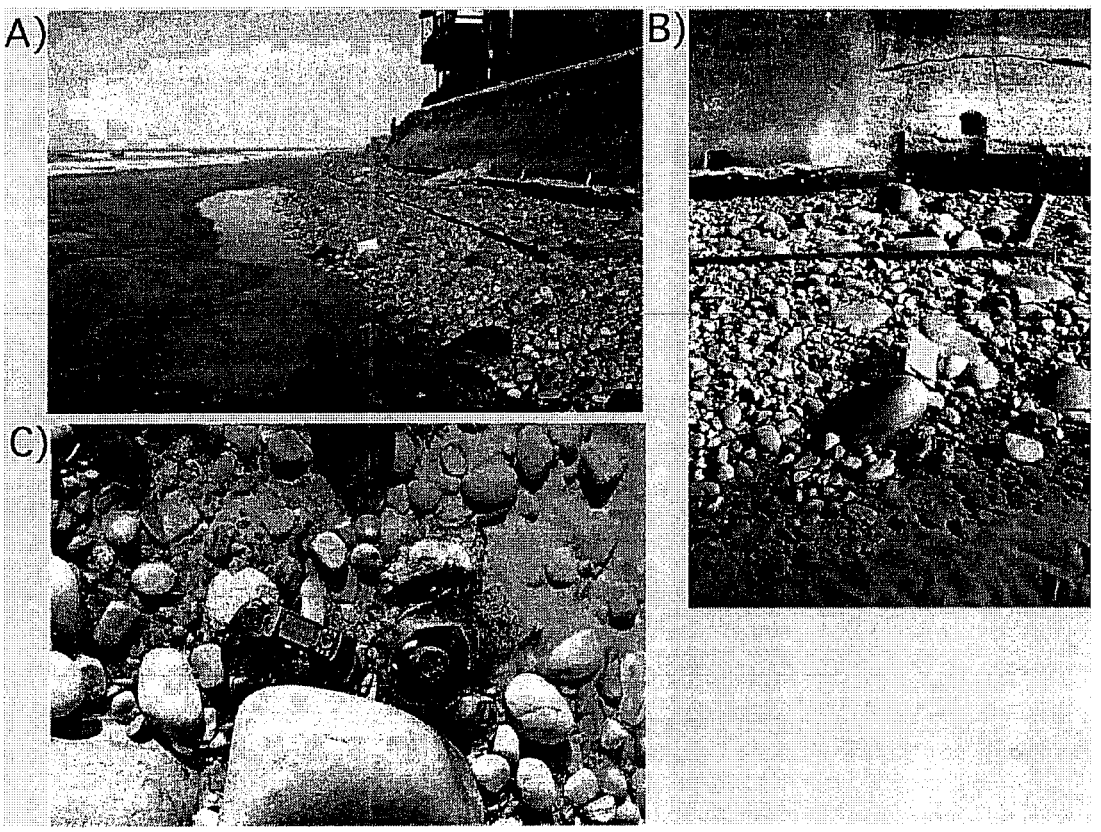

Fig. A3-3. A) and B) Sea wall at the west edge of the Summerland Beach. Small amounts of seepage was observed from the sea wall and from C) cutoff casings on the beach. Closeup of leaking oil casing. This casing is one of several on cobble beach near the base of the seawall at the west edge of the Summerland Beach. Small slick represents only a few drops of oil. Cobble beach and leaking casings are normally covered by at least one meter of sand. B) Note oil slick (lower right) in a tidal pool.

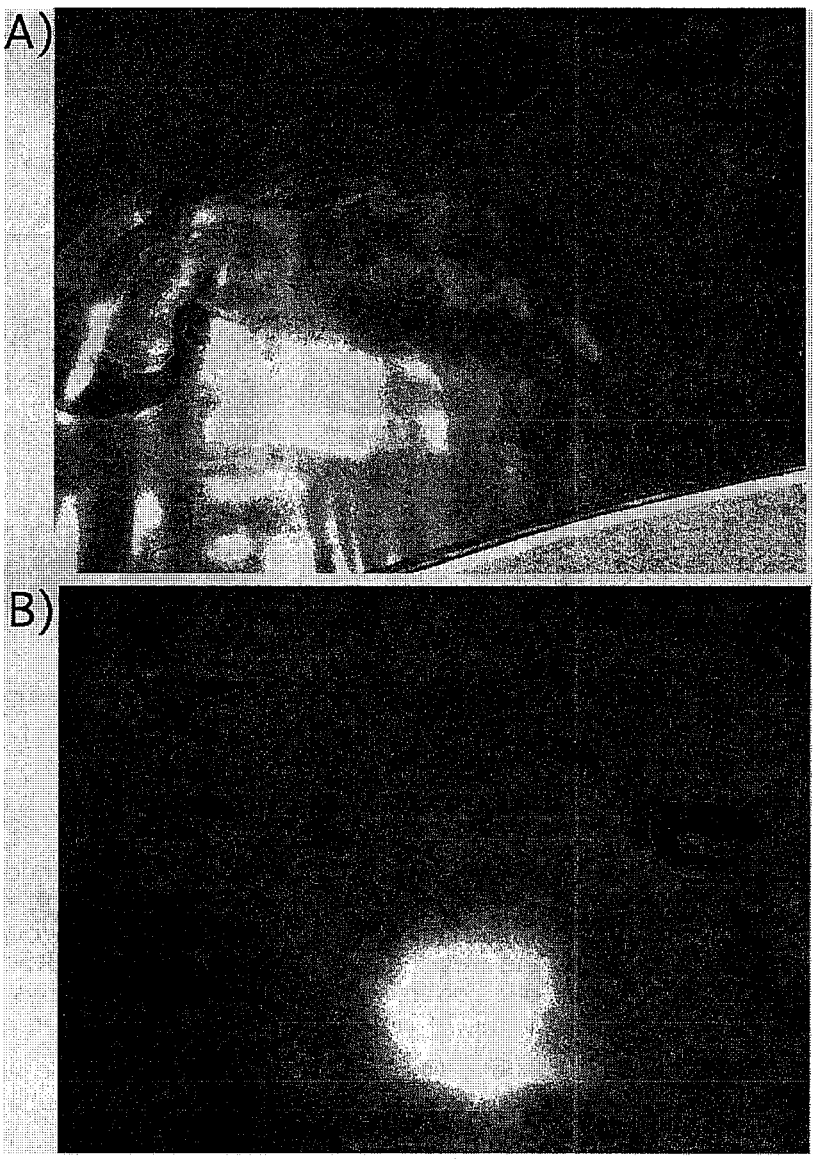

Fig. A3-4. Image of slick in nearshore Summerland waters. A) shows gunnel of boat. Slick color is due to the slick being an integer multiple of the wavelength of light.

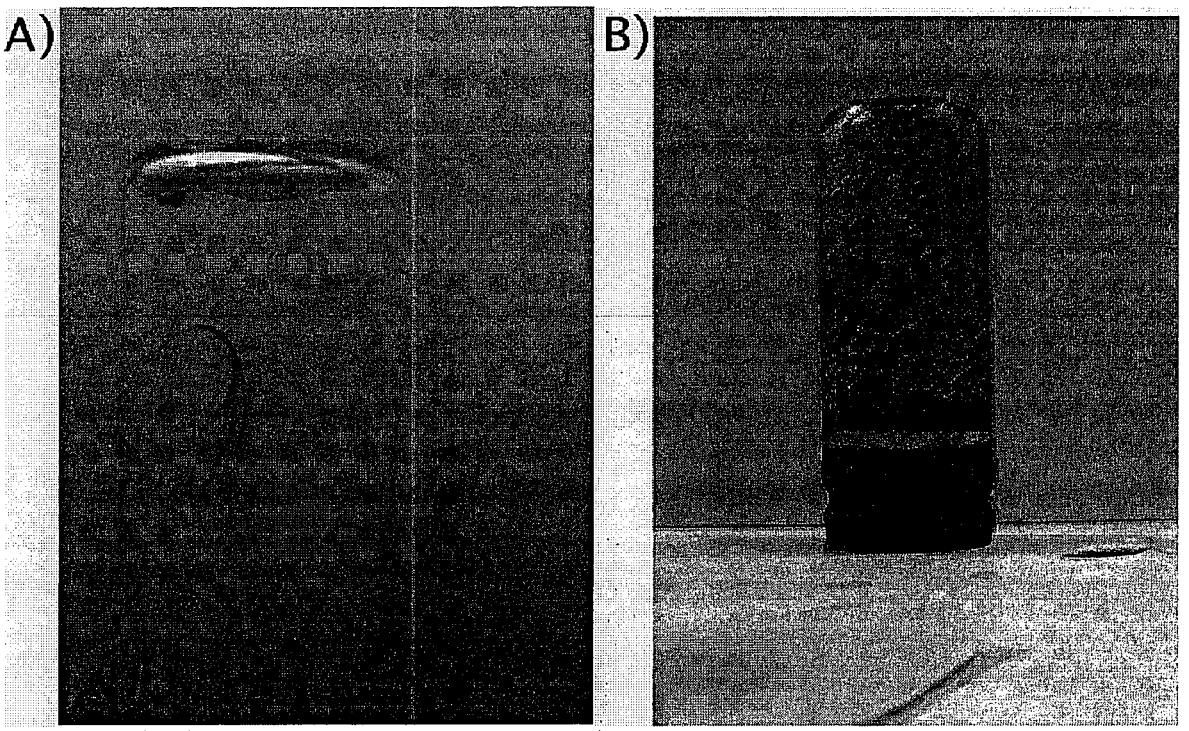

Fig. A3-5. A) Sample jar collecting oil and gas from Treadwell T-10 Well Site, and B) Full sample jar containing oil and gas.

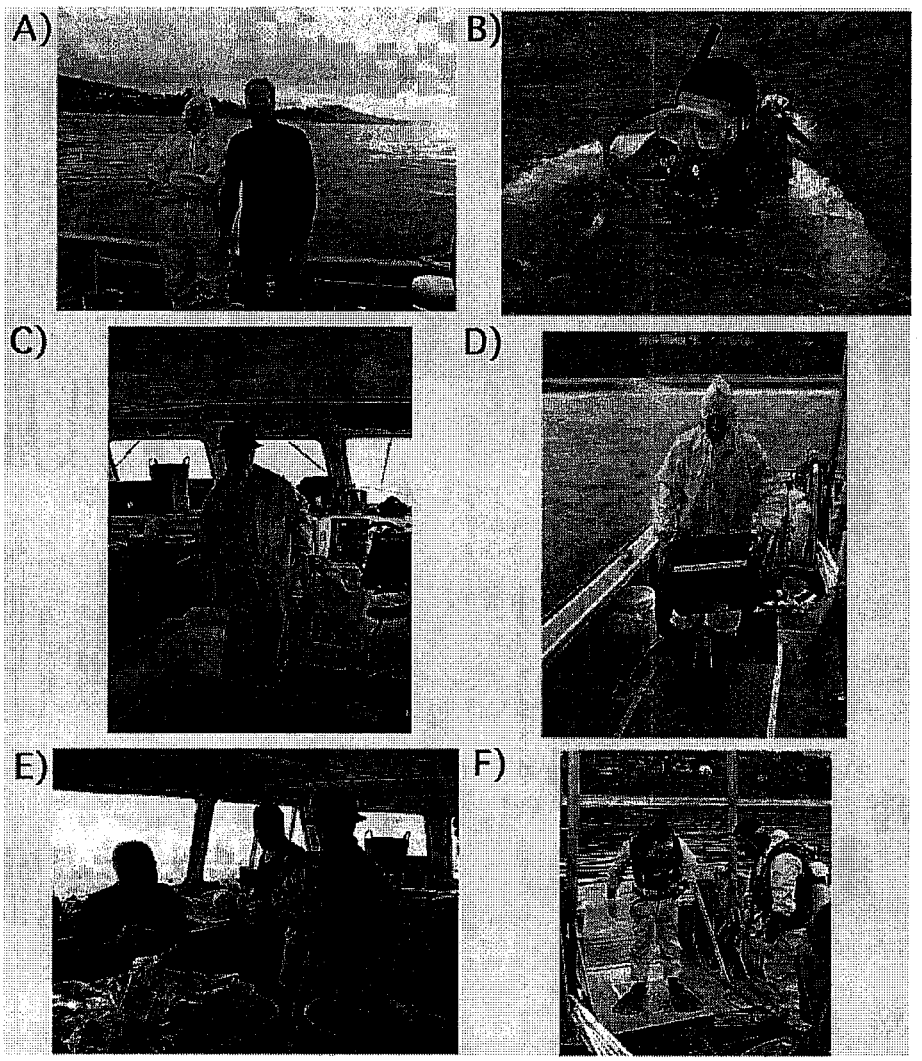

Fig. A3-6. Garibaldi photos. A) Tonya del Sontro and Dave Farrar B) Robin Lewis. C) Ken Wilson D) Ira Leifer E) Ray Michalski, Robin Lewis, and Ken Wilson F) Robin Lewis and Ian Taniguchi.

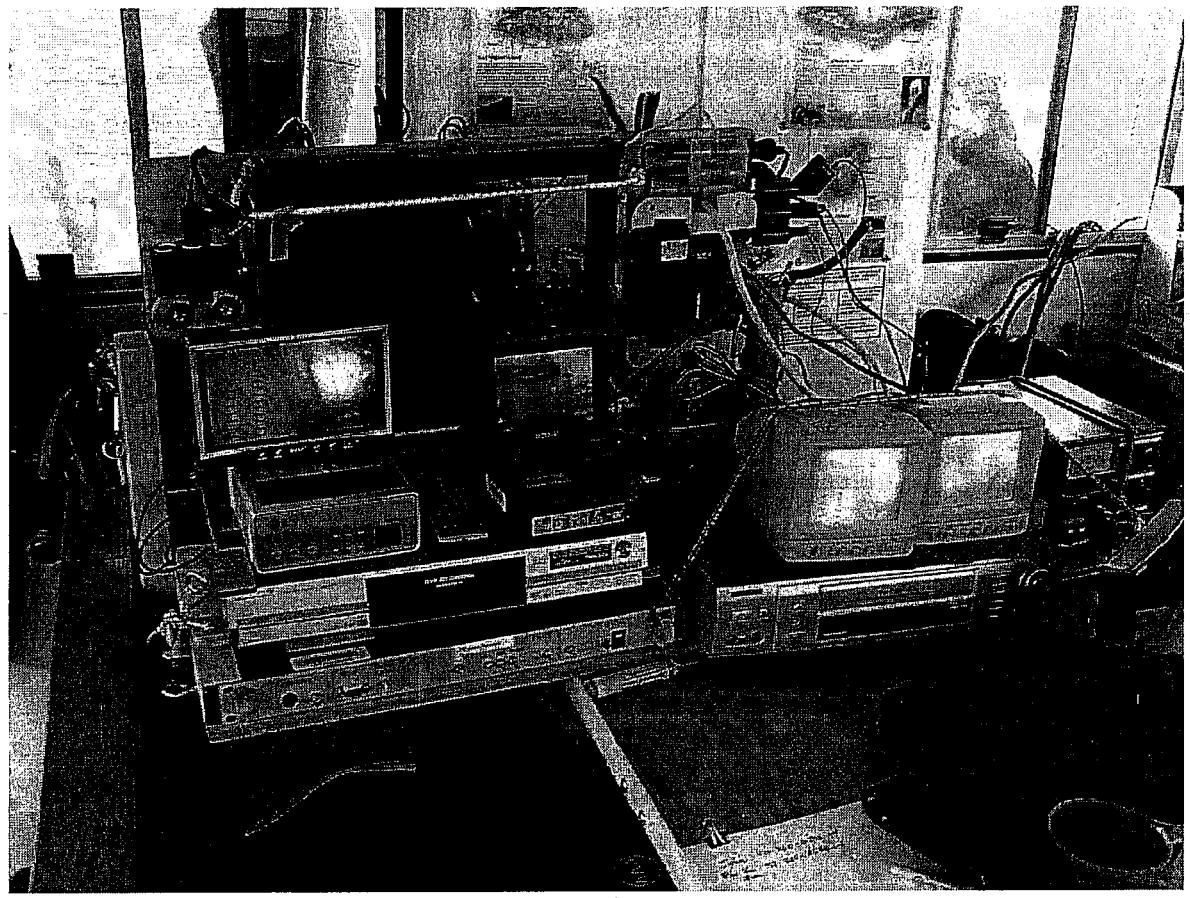

Fig. A3-7. Video monitors of seep tents on the California Department of Fish and Game, Marine Region's Research Vessel Garibaldi.

APPENDIX A4 – TIDE PREDICTION VERSUS LOCAL TIDE

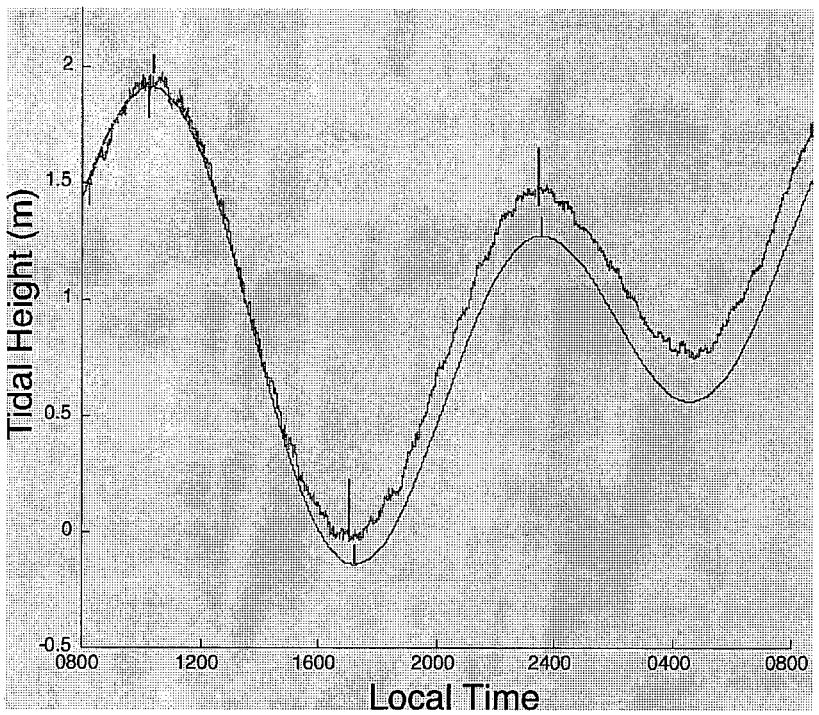

Fig. A4-1. Tide predictor versus measured tidal height for 18-19 Oct. 2005. The deviation (about 10 centimeters) in the measured depth was likely due to weather related changes in sea level. There also was a short 5 to 10 minute difference in the time of high and low tides (vertical bars) between the two. Thus, it is always better to measure tidal height.